The glycolytic enzyme PKM2 bridges metabolic and inflammatory dysfunction in coronary artery disease

Tsuyoshi Shirai,[1] Rafal R. Nazarewicz,[1,4] Barbara B. Wallis,[1] Rolando E. Yanes,[1] Ryu Watanabe,[1] Marc Hilhorst,[1] Lu Tian,[3] David G. Harrison,[4] John C. Giacomini,[2] Themistocles L. Assimes,[2] Jörg J. Goronzy,[1] and Cornelia M. Weyand[1]

[1]Division of Immunology and Rheumatology, Department of Medicine, [2]Division of Cardiovascular Medicine, Department of Medicine, and [3]Division of Biostatistics, Department of Health Research and Policy, Stanford University School of Medicine, Stanford, CA 94305
[4]Division of Clinical Pharmacology, Department of Medicine, Vanderbilt University School of Medicine, Nashville, TN 37232

Abnormal glucose metabolism and enhanced oxidative stress accelerate cardiovascular disease, a chronic inflammatory condition causing high morbidity and mortality. Here, we report that in monocytes and macrophages of patients with atherosclerotic coronary artery disease (CAD), overutilization of glucose promotes excessive and prolonged production of the cytokines IL-6 and IL-1β, driving systemic and tissue inflammation. In patient-derived monocytes and macrophages, increased glucose uptake and glycolytic flux fuel the generation of mitochondrial reactive oxygen species, which in turn promote dimerization of the glycolytic enzyme pyruvate kinase M2 (PKM2) and enable its nuclear translocation. Nuclear PKM2 functions as a protein kinase that phosphorylates the transcription factor STAT3, thus boosting IL-6 and IL-1β production. Reducing glycolysis, scavenging superoxide and enforcing PKM2 tetramerization correct the proinflammatory phenotype of CAD macrophages. In essence, PKM2 serves a previously unidentified role as a molecular integrator of metabolic dysfunction, oxidative stress and tissue inflammation and represents a novel therapeutic target in cardiovascular disease.

Cardiovascular disease remains the leading cause of death in the United States, and its prevalence is rapidly rising in developing countries. The underlying pathological process in coronary artery disease (CAD) is atherosclerosis, which was formerly considered a cholesterol deposition disease, but is now recognized to be a chronic inflammatory syndrome (Hansson and Hermansson, 2011; Witztum and Lichtman, 2014). Hypertension, smoking, diabetes, and obesity are well-established accelerators, but the molecular mechanisms are poorly understood. Conventional risk factor management leaves patients at high risk for heart attack or stroke, emphasizing the need for new strategies (Moore et al., 2013). A key pathogenic event is the recruitment of monocyte-derived cells into the subendothelial space, where they differentiate into macrophages, ingest lipids, turn into foam cells, remove debris and participate in efferocytosis. Plaque-residing macrophages secrete cytokines, enzymes, and growth factors, are cytotoxic, produce reactive oxygen species (ROS), and present antigen to T cells (Shirai et al., 2015). The clinical use of C-reactive protein (CRP) as a reliable biomarker for cardiovascular disease and its outcome assigns a particular role to the inflammatory cytokine IL-6, which is a major inducer of CRP (Ridker et al., 2008).

A typifying feature of macrophages is their plasticity and ability to respond to environmental cues (Martinez et al., 2013; Martinez and Gordon, 2014). Functional subsets are broadly classified into inflammatory M1 and tissue-reparative M2 macrophages with M1 polarization resulting from IFN-γ and TLR ligand exposure (Martinez et al., 2008). M1 macrophages dominate in the vulnerable shoulder of atherosclerotic lesions, whereas M2 macrophages reside in the adjacent adventitia (Stöger et al., 2012). In late atherosclerosis, M1 macrophages facilitate formation of the necrotic core and destabilize lesion. The role of microenvironmental signals versus cell-indigenous abnormalities in the genesis of pathogenic macrophages is unknown. Interestingly, monocytes that have not yet infiltrated the tissue may already respond to inflammatory stimuli. Specifically, in response to tissue injury caused by acute myocardial infarction, monocytes up-regulate expression of *CD14*, *LGALS1*, *ITGAM*, *CD163*, *IFN GR1*, *CYBB*, *CD93*, *DUSP6*, *IL13RA1*, *TLR2*, and several cell cycle genes (Ruparelia et al., 2015). Whether monocytes in at-risk individuals are more susceptible to activating stimuli is currently unknown.

Oxidative stress, as imposed by cigarette smoking, is a core risk factor for atherosclerosis (Fearon and Faux, 2009). ROS can damage proteins, carbohydrates, lipids, and DNA, but also function as second messengers to alter protein kinases, phosphatases, phospholipases, and transcription fac-

Correspondence to Cornelia M. Weyand: cweyand@stanford.edu

Abbreviations used: 2-DG, 2-deoxy-glucose; CAD, coronary artery disease; CRP, C-reactive protein; ECAR, extracellular acidification rate; HIF-1α, hypoxia-inducible factor-1α; mtROS, mitochondrial ROS; NAPDH, nicotinamide adenine dinucleotide phosphate-oxidase; NOX, NAPDH oxidase; OCR, oxygen consumption rate; PEP, phosphoenolpyruvate; PKM2, pyruvate kinase M2; ROS, reactive oxygen species.

The Rockefeller University Press $30.00
J. Exp. Med. 2016 Vol. 213 No. 3 337–354
www.jem.org/cgi/doi/10.1084/jem.20150900

tors (Liu et al., 2005). H_2O_2 imposes its regulatory control through reversible oxidization of cysteine residues. ROS are an inevitable byproduct of the mitochondrial electron transfer and, as such, directly relate to metabolic activity (Korge et al., 2008). Immune cells, including macrophages, depend on glycolysis as a major energy source (O'Neill and Hardie, 2013; Colegio et al., 2014; Huang and Pearce, 2014). In recent studies, metabolic intermediates have been suggested to regulate IL-1β production in macrophages, e.g., succinate stabilizes hypoxia-inducible factor-1α (HIF-1α), driving production of IL-1β, but not IL-6 or TNF (Tannahill et al., 2013). Importantly, the glycolytic enzyme pyruvate kinase M2 (PKM2) also controls HIF-1α activity, and thus IL-1β induction (Palsson-McDermott et al., 2015).

Glucose metabolism of lesion-residing macrophages is up-regulated, such that atherosclerotic lesions can be visualized by positron emission tomography using 18F-fluorodeoxyglucose (Rudd et al., 2002). Abnormal glucose metabolism is a core aspect of metabolic syndrome; a cluster of conditions associated with high risk for heart disease, stroke and diabetes (Grundy et al., 2004). Here, we directly implicate excess glucose utilization in pathogenic monocyte and macrophage functions and chronic inflammation. We find that monocytes from CAD patients are prone to differentiate into IL-6 and IL-1β–producing effector cells, and maintain this property as they differentiate into macrophages. This hyperinflammatory state is mechanistically dependent on glycolytic activity and glucose-induced ROS production by the mitochondria. ROS production within macrophages changes the oligomeric assembly of the redox-sensing enzyme PKM2, enabling its nuclear import and phosphorylation of STAT3, to promote IL-6 and IL-1β production. Our results indicate that PKM2 is a previously unidentified pinnacle checkpoint that connects glucose overutilization to inflammatory effector functions, marking this metabolite and nuclear kinase as a novel therapeutic target to correct aberrant inflammatory immune responses in atherosclerosis.

RESULTS

Circulating monocytes in CAD patients are hyperinflammatory

To understand how monocytes and macrophages contribute to inflammatory pathology in CAD, we analyzed the distribution of monocyte subsets in CAD patients and age-matched healthy individuals. Patients had reduced frequencies of classical $CD14^{++}CD16^{-}$ monocytes, and instead expanded the intermediate $CD14^{++}CD16^{+}$ subset (Fig. 1, A and B). Elevated numbers of intermediate monocytes have been proposed to predict cardiovascular events (Rogacev et al., 2012). The relatively small population of nonclassical monocytes was similar in both study cohorts.

Gene expression profiling of freshly isolated monocytes revealed that patient-derived cells were poised to produce IL-6 and IL-1β, as well as the chemokine CCL18 (Fig. 1 C). To investigate how the shift in monocyte subsets and the altered gene expression in patient-derived cells may ultimately impact macrophage effector functions, we isolated $CD14^{++}CD16^{-}$ and $CD14^{++}CD16^{+}$ cells by fluorescence-activated cells sorting, differentiated them into macrophages and analyzed their cytokine production. As shown in Fig. 1 D, macrophages originating from the intermediate monocyte population produced significantly higher amounts of IL-1β, IL-6, and TNF, confirming that these cells are biased toward inflammatory effector functions.

Hyperinflammatory CAD M1 macrophages produce excess IL-6 and IL-1β

In the atherosclerotic plaque, monocytes recruited from the circulation differentiate into macrophages in response to local macrophage colony-stimulating factor before they display their proatherogenic functions (Hansson and Libby, 2006). To test whether reprogrammed CAD monocytes memorize their bias toward inflammatory cytokine production upon entering the tissue space, we first compared ex vivo–differentiated macrophages from patients and controls. Macrophages were polarized toward the M1 or M2 phenotype and gene expression profiles were analyzed (Fig. 2 A). Patient-specific signatures in M1 macrophages, defined as a greater than fourfold difference in gene expression, included the proinflammatory cytokines IL-6 and IL-1β, the chemokine CCL18, and multiple chemokine receptors (CCR1, CCR2, CXCR4, CCR7, and CCR5). Expression of IL-6 and IL-1β was markedly increased in CAD patients, but TNF expression was indistinguishable between cases and controls. Krüppel-like factor 2 and 4, negative regulators of inflammatory genes (Mahabeleshwar et al., 2011), were significantly down-regulated in patient-derived cells. Similar to the findings in monocytes (Fig. 1 C), expression of NAD(P)H:quinone oxidoreductase1, a target gene of the ROS-sensitive transcription factor NF-E2–related factor 2 (Itoh et al., 2010), was strikingly increased in patient macrophages, suggesting that the cells are under oxidative stress.

The cytokine production potential was confirmed by staining of intracellular cytokine stores. Macrophage activation induced down-regulation of CD14 (Fig. 2 B). In healthy individuals, $CD14^{low}$ macrophages accounted for 20–30%, but in CAD patients, the $CD14^{low}$ population was doubled in resting and stimulated populations (Fig. 2 C). Cytokine production was predominantly a feature of $CD14^{low}CD11b^{high}$ $CD16^{low}$ cells (Fig. 2 D). TLR4 expression was similar in all macrophage populations (unpublished data).

Macrophages poised to produce IL-6 and IL-1β were markedly increased in CAD patients (Fig. 2, E and F), confirming the gene expression data. Kinetic studies after stimulation demonstrated significantly higher frequencies of IL-1β–producing macrophages in the patients at 6 h. Differences in control and CAD macrophages were most pronounced for IL-6, an important biomarker of cardiovascular risk (Ridker et al., 2000). Less than 20% of stimulated healthy macrophages synthesized IL-6 (Fig. 2 G). Conversely, CAD macrophages

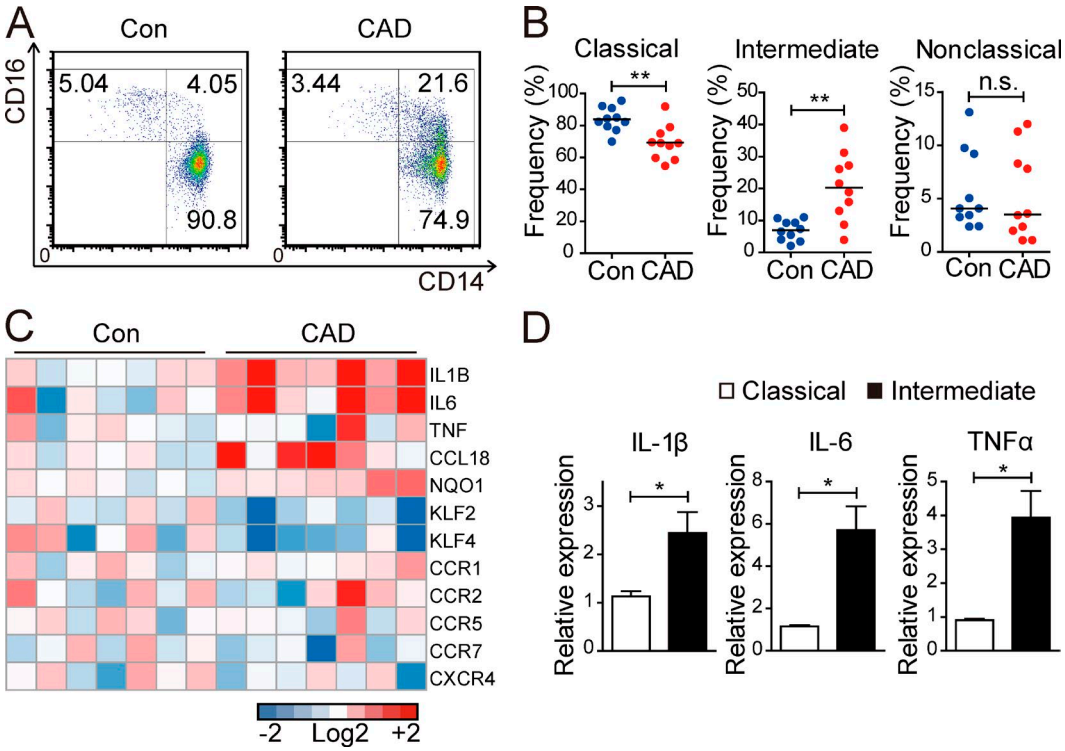

Figure 1. **Hyperinflammatory monocytes in CAD patients.** PBMCs isolated from healthy controls and CAD patients were stained with CD14, CD16, and HLA-DR, and frequencies of monocyte subsets were measured by flow cytometry. Representative dot plots (A) and frequencies of the three monocyte subpopulations (B) are shown. (C) Monocytes from seven controls and seven CAD patients were stimulated with LPS/IFN-γ, and RNA expression of genes was measured by quantitative RT-PCR. Heat map displays expression of genes with data presented as the $\log_2$ value. (D) Classical and intermediate monocytes were sorted by flow cytometry, differentiated into macrophages, and stimulated with LPS/IFN-γ, and then cytokine RNA expression was measured by RT-PCR ($n = 6$). Values are mean ± SEM. *, $P < 0.05$; **, $P < 0.01$.

rapidly produced IL-6, with 30–40% of stimulated cells laden with IL-6 protein. Frequencies of TNF^+ macrophages were indistinguishable in patients and controls. Cytokine production by $CD14^{high}$ macrophages was similar in all study cohorts.

To control for the possible effect of medications frequently taken by CAD patients, we recruited healthy individuals taking aspirin, statins, β-blockers, or ACE inhibitors. Frequencies of IL-1β–, IL-6–, or TNF-producing macrophages were essentially unaffected by exposure to such drugs (Fig. 2 H). Macrophages were cultured in relevant doses of aspirin, lisinopril, simvastatin, or metoprolol, and none of these drugs increased IL-6 and IL-1β production beyond the level of untreated cells (unpublished data).

In essence, monocytes in CAD patients are committed to the production of proinflammatory cytokines, and most of the abnormalities persist once cells have differentiated into macrophages. In macrophages, excess cytokine production is selective for IL-6 and IL-1β, whereas TNF production is indistinguishable in CAD and controls.

IL-6–producing macrophages in CAD

To seek for a role of $IL\text{-}6^+$ macrophages in the disease process, we first localized IL-6–containing tissue macrophages in the atherosclerotic plaque (Fig. 3 A). Also, the frequency of $IL\text{-}6^+$ macrophages induced ex vivo correlated with high-sensitivity CRP measurements in the donor patient (Fig. 3 B), suggesting that IL-6 release by such effector cells contributes to the systemic inflammatory syndrome of CAD. Correlative studies of the frequencies of $IL\text{-}6^+$ macrophages in individual patients with clinical parameters demonstrated significantly higher frequencies in patients that had diabetes mellitus type 2, hypertension, or hyperlipidemia, all considered risk factors for coronary events (Fig. 3, C and D). Most importantly, frequencies of $IL\text{-}6^+$ macrophages increased progressively with the presence of one, two, or three comorbidities, suggesting additive effects of each risk factor.

Excess IL-6 and IL-1β generation is ROS dependent

NAD(P)H:quinone oxidoreductase 1 up-regulation in CAD monocytes and macrophages suggested increased oxidative stress (Fig. 1 C and Fig. 2 A), which was confirmed by quantification of intracellular ROS levels (Fig. 4, A–C). Compared with healthy controls, CAD monocytes generated significantly higher ROS concentrations in resting as well as activated cells (Fig. 4 A). In patient-derived macrophages, ROS levels were

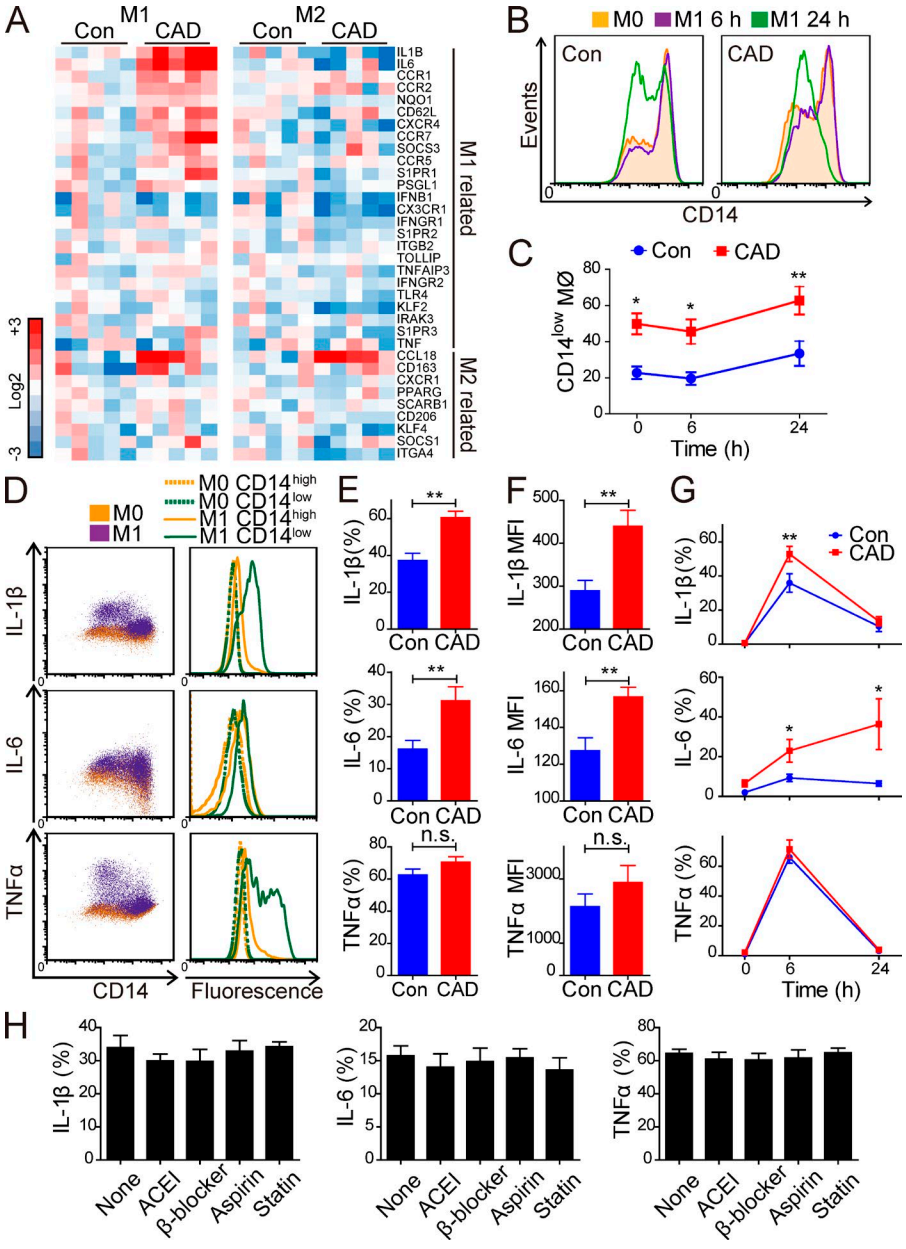

Figure 2. **CAD macrophages produce excessive IL-6 and IL-1β.** (A) Monocytes were isolated from five healthy controls and five CAD patients, differentiated into macrophages using macrophage colony-stimulating factor (M-CSF) and polarized into M1 and M2 cells. Gene expression was measured using quantitative RT-PCR. Heat map displays expression of genes with data presented as the $\log_2$ values. (B) Macrophages from healthy controls and CAD patients were stimulated with LPS/IFN-γ for 6 and 24 h. CD14 expression was analyzed by flow cytometry. Representative histograms are shown. (C) Frequencies of $CD14^{low}$ macrophages in five healthy controls and five CAD patients at indicated time points after stimulation. (D) Production of IL-1β, IL-6, and TNF was measured by intracellular staining using flow cytometry in M0 (dashed lines) and M1 macrophages (solid lines). Percentage of cytokine producing macrophages (E) and mean fluorescent intensities (MFI) of intracellular cytokine stains (F) in the $CD14^{low}$ population 6 h after LPS/IFN-γ stimulation (15 controls [blue] and 16 CAD patients [red]). (G) Cytokine production at the indicated time points after LPS/IFN-γ stimulation assessed by intracellular cytokine staining in healthy controls (blue; $n = 8$) and CAD patients (red; $n = 7$). (H) Frequencies of cytokine-producing macrophages were compared in healthy individuals not taking medications ($n = 14$) and those taking the indicated medications ($n = 5$ per treatment). Values are mean ± SEM. *, $P < 0.05$; **, $P < 0.01$.

doubled compared with controls (Fig. 4, B and C). To examine the relationship between aberrant ROS generation and cytokine production, cells were pretreated with the superoxide dismutase mimetic Tempol (Wilcox, 2010). Scavenging superoxide reduced IL-6 and IL-1β production, whereas TNF remained unaffected (Fig. 4, D and E). These data implicated superoxide or one of its products, such as peroxynitrite, in promoting macrophage inflammatory effector functions.

ROS derive from several cellular sources, foremost nicotinamide adenine dinucleotide phosphate-oxidases (NOX) and mitochondria (Nathan and Cunningham-Bussel, 2013). NOX2 is the predominant isoform in human macrophages (Fig. 4 F). Neither NOX2 knockdown by RNA interference (Fig. 4, G and H) nor NOX2 assembly inhibition by gp91dstat (Rey et al., 2001; Fig. 4 I) affected cytokine production; eliminating NOX-derived ROS as relevant in regulating the inflammatory phenotype of CAD macrophages. Pretreatment with Mitotempo, a mitochondria-target ROS scavenger (Dikalova et al., 2010), significantly reduced the frequencies of IL-6– and IL-1β–producing macrophages without changing TNF production (Fig. 4, J and K), suggesting that mitochondria control the inflammatory behavior of macrophages in cardiovascular disease.

Glucose fuels the excess ROS production

Cellular ROS are a byproduct of the mitochondrial respiratory chain, conveying signals from multiple substrates, including glycolysis-derived pyruvate. We deprived the cells of

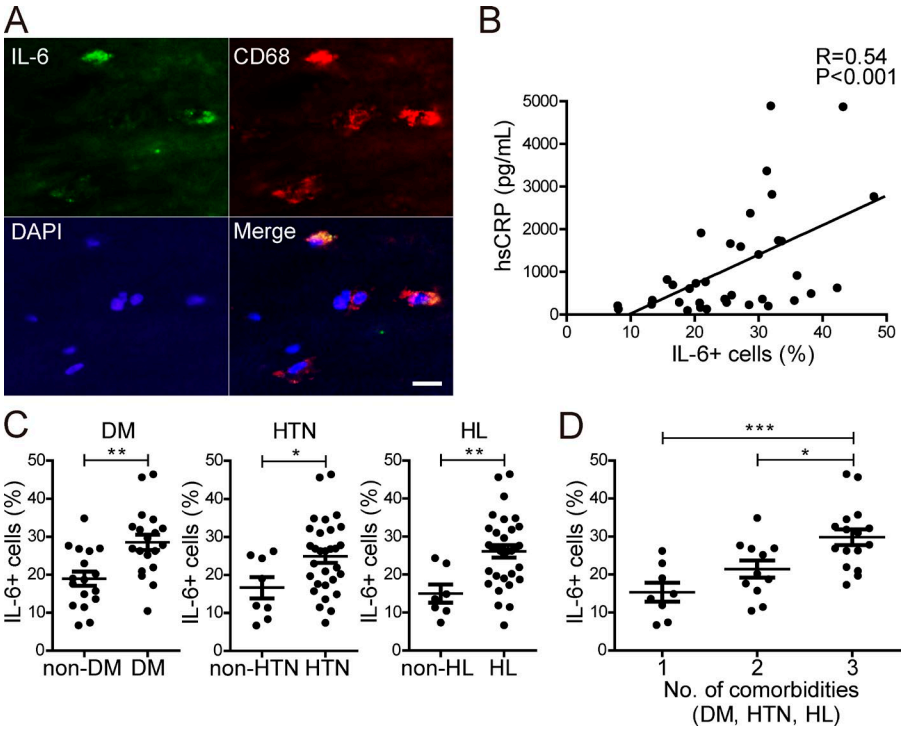

Figure 3. **IL-6–producing macrophages in patients with CAD.** (A) Frozen sections of carotid atheromas were immunostained with anti-IL-6 (green), anti-CD68 (red), and DAPI (blue), and analyzed by fluorescence microscopy. One representative of three independent experiments. Bar, 20 µm. (B) Plasma high-sensitivity CRP (hsCRP) is correlated with the frequency of ex vivo–generated IL-6–producing macrophages for each individual patient. (C) Patients are stratified according to the absence and presence of type 2 diabetes mellitus (DM), hypertension (HTN), and hyperlipidemia (HL). Each symbol represents the frequency of IL-6–producing macrophages from each individual patient. (D) The frequency of IL-6–producing macrophages in each individual patient is correlated with the number of comorbidities (DM, HTN, or HL). *, $P < 0.05$; **, $P < 0.01$; ***, $P < 0.001$.

glucose using 2-deoxy-glucose (2-DG), a glucose analogue that inhibits hexokinase and phosphoglucose isomerase (Ralser et al., 2008). 2-DG treatment for 6 h did not affect the viability of macrophages, but significantly decreased IL-6 and IL-1β production, whereas TNF appeared to be glucose independent (Fig. 5, A, B, and E). Similarly, removal of exogenous glucose attenuated IL-6 and IL-1β, but not TNF, induction (Fig. 5, C and D). Glucose restriction (2-DG) and ROS scavenging (Tempol) effectively diminished IL-6 and IL-1β transcripts concentrations (Fig. 5 F), suggesting that ROS interfere with transcriptional regulation of cytokines.

To test whether monocytes and macrophages of CAD patients are prone to use more glucose, glucose uptake was quantified in resting and activated monocytes (Fig. 5 G) and in resting and activated macrophages (Fig. 5 H). Glucose uptake was significantly enhanced in patient-derived cells. To mechanistically link glucose uptake and ROS production, we measured mitochondrial ROS (mtROS) with the mitochondria-targeted MitoSOX probe (Fig. 5 I). Levels of mtROS were directly correlated to the dose of glucose taken up by the cell (Fig. 5 I).

Higher mitochondrial activity in CAD monocytes and macrophages was confirmed by Seahorse extracellular flux assays (Fig. 6). Oxygen consumption rates (OCRs) and extracellular acidification rates (ECARs) were analyzed 3 h after stimulation with LPS/IFN-γ, timed such that mitochondrial function was assessed while the cells were producing cytokines. Activated CAD monocytes and macrophages were distinguished from control cells by significantly higher OCR. After uncoupling, patient-derived cells were able to use oxygen much more effectively than controls (Fig. 6, A and D), which is indicative of a higher respiratory reserve capacity and suggests the presence of adaptive mechanisms preparing the mitochondria for higher substrate load. In parallel, patient-derived cells had up-regulated glycolytic flux and generated more lactate, as indicated by higher ECAR (Fig. 6, B and E). Because both ECAR and OCR were elevated in patients, the ECAR/OCR ratio was indistinguishable between cases and controls (Fig. 6, C and F).

These results identified glucose uptake as an upstream event in the functional abnormalities of CAD monocytes and macrophages and mechanistically linked excess glucose utilization and tight coupling of the mitochondrial electron transport chain to oxidative stress.

CAD macrophages overexpress the glycolytic enzyme PKM2

Gene expression profiling revealed that M1 polarized macrophages from CAD patients overexpressed eight genes required for glucose uptake and breakdown (*PKM2*, *GLUT3*, *PDK1*, *PFKFB3*, *HK2*, *PGK1*, *PFK1*, and *GLUT1*; Fig. 7 A), as well as the two glycolytic master regulators c-Myc and HIF-1α. In M2-polarized cells from patients and controls, glycolysis-related genes were low in abundance and expressed at indistinguishable levels between the two groups. Based on transcript levels, GLUT1 was by far the dominant glucose transporter in macrophages, followed by a fivefold lower transcript level for GLUT3. Essentially, no transcripts were found for the insulin-dependent GLUT4 transporter or GLUT2 (Fig. 7 B).

PKM2, one of the isoforms of the enzyme that catalyzes the final step of glycolysis and converts phospho-

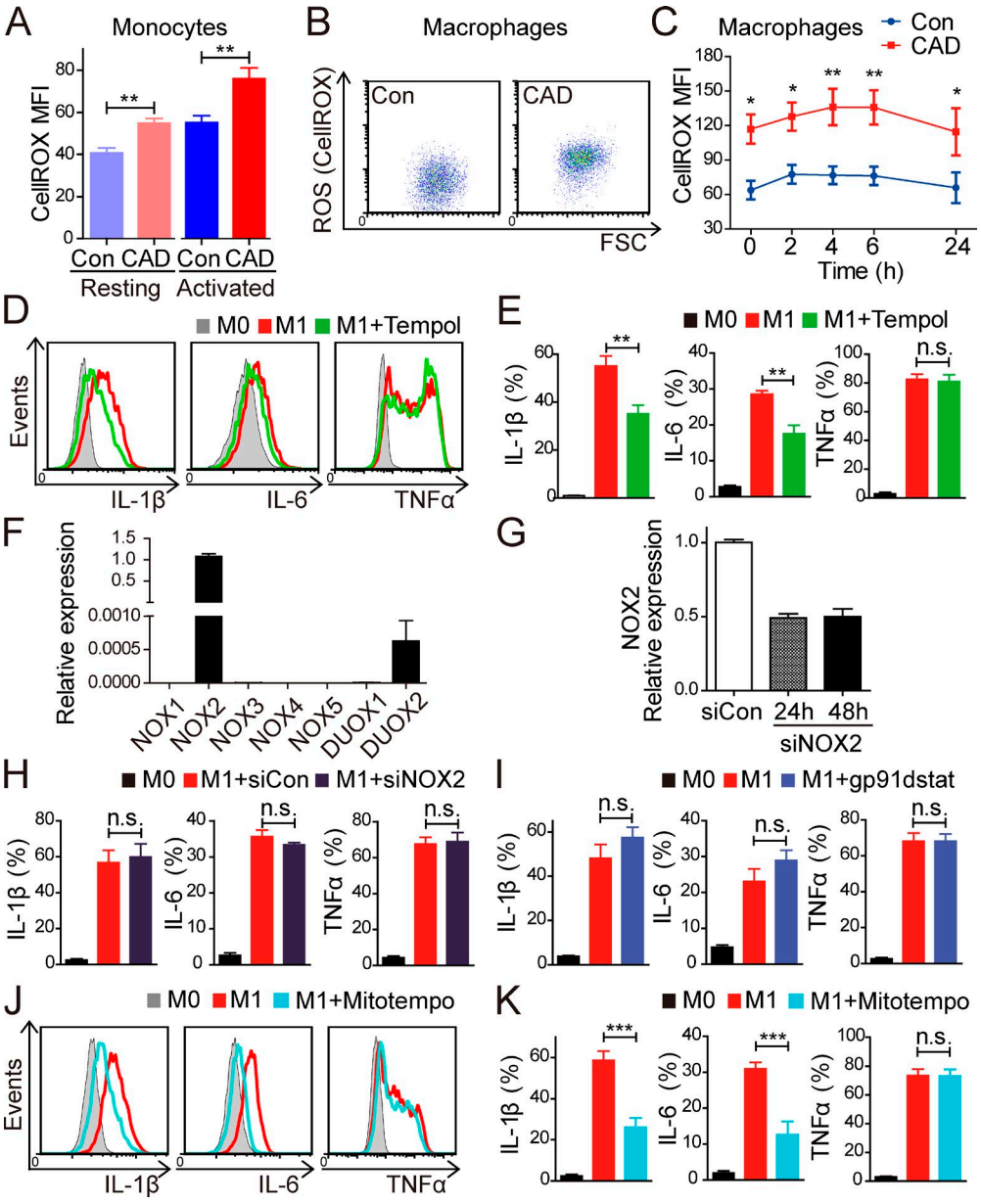

Figure 4. **ROS scavenging corrects the inflammatory phenotype of CAD macrophages.** (A) Resting or activated monocytes were loaded with 5 µM CellROX Deep Red and intracellular ROS levels were analyzed by flow cytometry. Summarized mean fluorescent intensities (MFI) from $n = 10$ healthy controls and $n = 10$ CAD patients are shown. (B and C) Macrophages from controls and CAD patients were stimulated with LPS/IFN-γ for 2, 4, 6, and 24 h. Cells were then loaded with CellROX Deep Red and intracellular ROS levels were analyzed by flow cytometry. Representative dot plots (B) and MFI from macrophages of $n = 7$ healthy controls and $n = 7$ CAD patients (C) are shown. (D and E) CAD macrophages were stimulated for 6 h under M1-polarizing conditions in the absence (red) and presence (green) of the ROS scavenger Tempol (50 µM) and intracellular cytokines were measured by flow cytometry. (F) Total RNA was purified from ex vivo–generated macrophages, and expression of NOXs was measured by qRT-PCR ($n = 3$). (G) Macrophages were transfected with either siControl RNA or siNOX2 RNA, and total RNA was purified at the indicated times. NOX2 expression was measured by qRT-PCR ($n = 3$). (H) CAD macrophages were transfected with control or NOX2 siRNA and intracellular cytokines were measured by flow cytometry after 6 h of stimulation ($n = 5$). (I) CAD macrophages were stimulated in the absence and presence of gp91dstat (50 µM). Intracellular cytokines were measured by flow cytometry ($n = 5$). (J and K) CAD macrophages were treated with or without Mitotempo (20 µM). Intracellular cytokines were analyzed after 6 h of stimulation ($n = 6$). All data are mean ± SEM. *, $P < 0.05$; **, $P < 0.01$; ***, $P < 0.001$.

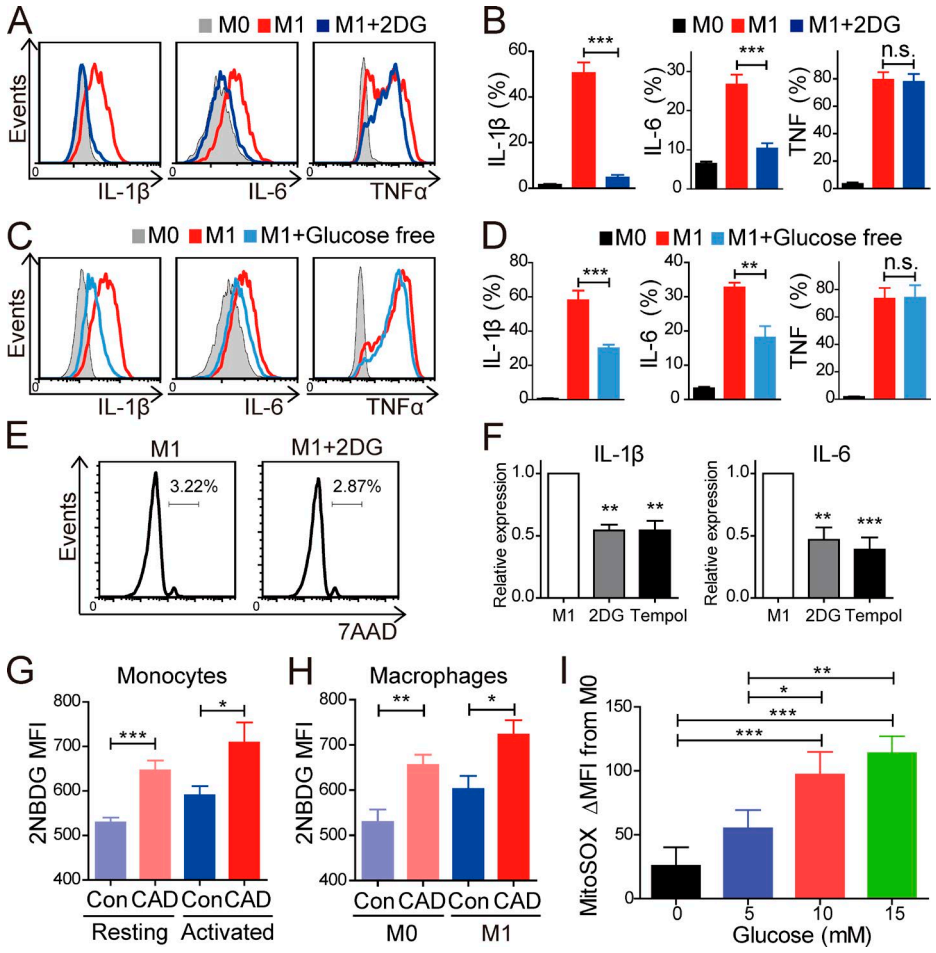

Figure 5. **Glucose deprivation disrupts proinflammatory effector functions and ROS production.** M0 macrophages were generated from CAD patients, stimulated with LPS/IFN-γ for 6 h and intracellular cytokines were measured by flow cytometry. Glycolytic activity was suppressed with 10 mM of 2-DG (A and B) or glucose-free medium (C and D). Representative histograms of intracellular cytokine stains and frequencies of cytokine-producing macrophages from five independent experiments are shown. (E) CAD macrophages were stimulated with LPS and IFN-γ for 6 h in the absence or presence of 10 mM of 2-DG. Macrophages were then stained with 7-AAD and viability of cells was measured by flow cytometry. Representative histograms from four independent experiments are shown. (F) CAD macrophages were stimulated with LPS and IFN-γ for 6 h in the absence or presence of 10 mM of 2-DG or 50 µM of Tempol. Expression of IL-1β and IL-6 was measured by qRT-PCR ($n = 4$). (G) Glucose uptake in monocytes was measured using the fluorescence-labeled glucose analogue, 2-NBDG. Summarized MFI from 12 independent experiments are shown. (H) Glucose uptake in macrophages was measured using the 2-NBDG. Summarized MFI from 10 independent experiments are shown. (I) Macrophages from CAD patients were stimulated for 4 h, and loaded with 5 µM of MitoSOX to quantify mtROS levels. Data represent ΔMFI compared with resting cells from four independent experiments. All data are mean ± SEM. *, $P < 0.05$; **, $P < 0.01$; ***, $P < 0.001$.

enolpyruvate (PEP) to pyruvate (Noguchi et al., 1986), is typically expressed in tumor cells (Christofk et al., 2008a). We found that PKM2 is also the dominant isoform in human macrophages (Fig. 7 C). Confocal microscopy demonstrated abundant expression of PKM2 protein in control macrophages and even higher levels in CAD macrophages (Fig. 7 D). Healthy cells contained an evenly distributed pattern of cytoplasmic PKM2. In CAD macrophages, however, PKM2 assembled in a punctate pattern, with perinuclear dominance and nets distributed throughout the nucleus. Quantification of the nuclear signal demonstrated that CAD nuclei consistently contained more PKM2 protein than control cells (Fig. 7, D and E).

To verify the importance of PKM2 in CAD, we evaluated PKM2 expression in atheromatous lesions. PKM2 was found in all atherosclerotic plaques, almost entirely localizing to $CD68^+$ macrophages (Fig. 7 F).

These data identified PKM2 as a constitutive element in atheroma-related macrophages and raised the question of the enzyme's cytoplasmic versus nuclear functions.

PKM2 dimerization in CAD monocytes and macrophages

PKM2 can change its oligomeric status, ranging from metabolically low-activity monomeric and dimeric forms to metabolically high-activity tetrameric forms. Among glycolytic enzymes, the oligomeric PKM2 stands out as a redox-sensitive

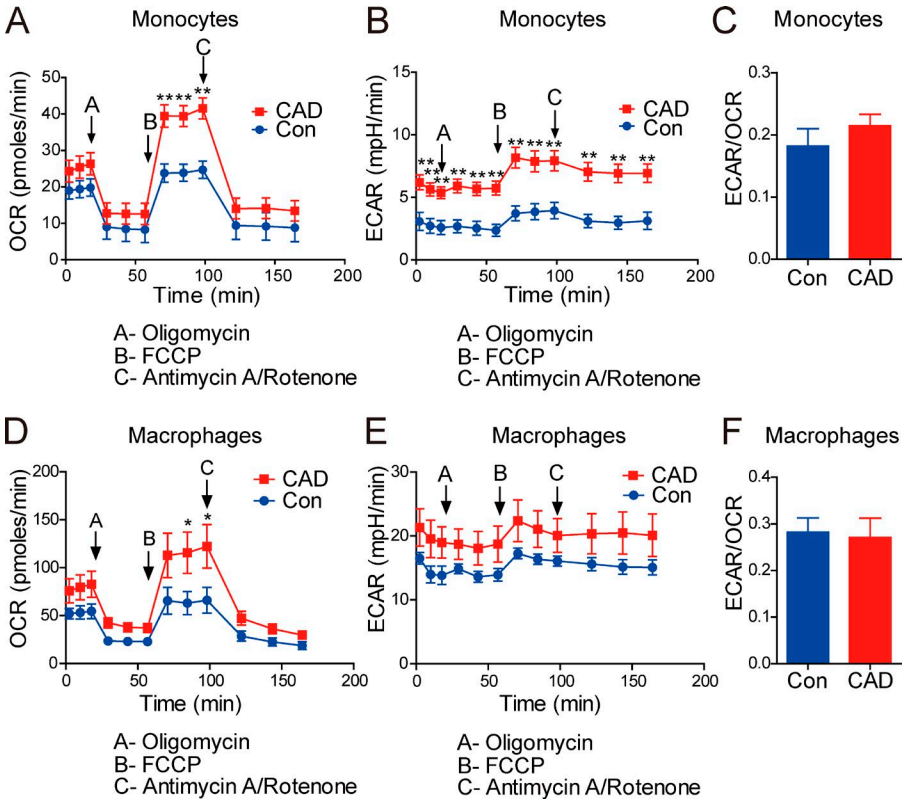

Figure 6. **Mitochondrial respiration and glycolysis assays in monocytes and macrophages.** (A–C) OCRs (A) and ECARs (B) were measured with the Seahorse Bioscience XF96 analyzer in monocytes 3 h after LPS/IFN-γ stimulation. Summarized graph from seven healthy controls and eight CAD patients is shown. Mitochondrial function was probed by the serial addition of oligomycin, FCCP, and antimycin A/rotenone as indicated. (C) ECAR-OCR ratios in controls and CAD patients. (D–F) OCR (D) and ECAR (E) were determined with the Seahorse Bioscience XF96 analyzer in macrophages 3 h after LPS/IFN-γ stimulation. Summarized graph from four healthy controls and six CAD patients is presented. Oligomycin, FCCP, and antimycin A/rotenone were added serially as in A and B. (F) ECAR-OCR ratios calculated for controls and patients. All data are mean ± SEM. *, $P < 0.05$; **, $P < 0.01$.

molecule (Anastasiou et al., 2011). Dimeric PKM2 has low pyruvate kinase activity and, in cancer cells, can enter the nucleus (Gao et al., 2012), whereas tetrameric PKM2 is highly active in converting PEP to pyruvate. In contrast to murine macrophages, in which monomers are the predominant isoform (Palsson-McDermott et al., 2015), human monocytes and macrophages mostly contain dimeric PKM2 (Fig. 8, A–D). In control monocytes, PKM2 protein levels were low, with no detectable tetramers. In contrast, CAD monocytes spontaneously contained PKM2 expression levels, which were doubled, most of the protein in dimeric form (Fig. 8, A and B). PKM2 protein expression was markedly higher in macrophages (Fig. 8, C and D). Resting CAD macrophages had detectable PKM2 tetramers, which were lost after activation. Also, monomeric PKM2 was barely detectable in healthy macrophages, but was present in CAD macrophages (Fig. 8 C). Consistently, CAD monocytes and macrophages possessed significantly higher amounts of dimeric PKM2 compared with control cells (Fig. 8, B and D). Parallel to the activation-induced ROS increase (Fig. 4, B and C), LPS/IFN-γ stimulation shifted PKM2 into the nucleus, as demonstrated by confocal microscopy and Western blotting (Fig. 8, E–G). ROS scavenging prevented the enzyme's nuclear import. Impairing glycolytic activity with 2-DG essentially trapped PKM2 in the cytoplasm (Fig. 8 G). Thus, ROS induced by macrophage activation promptly changed the molecule's oligomeric state, down-regulating metabolically active tetramers. Conversely, Tempol or 2-DG treatment stabilized the tetrameric configuration, prevented dimerization, and effectively blocked nuclear translocation (Fig. 8 H).

To examine the impact of PKM2's oligomeric status on cytokine production, we enforced PKM2 tetrameric assembly with the small molecule ML265 (Walsh et al., 2010), which excludes the enzyme from the nucleus (Fig. 8, I and J). ML265 significantly suppressed production of IL-6 and IL-1β, but not of TNF. These results linked the inflammatory phenotype of CAD macrophages to PKM2's oligomeric state and subcellular localization and implicated glucose utilization and ROS in regulating the dimer/tetramer ratio of the enzyme.

Glycolysis and ROS promote STAT3 phosphorylation via PKM2 dimerization

The selectivity for IL-6 and IL-1β, but not TNF, guided the search for mechanisms downstream of PKM2 nuclear translocation. PKM2 directly interacts with HIF-1α, promoting transactivation of HIF-1 target genes (Luo et al., 2011). Consistent with Tannahill et al. (2013), HIF-1α inhibition reduced IL-1β, but IL-6 and TNF production were unaffected (Fig. 9 A), eliminating HIF-1α as the main regulator of IL-6 and IL-1β in CAD macrophages. IL-6 and IL-1β promoters share binding sites for STAT3, which is not implicated in TNF transcription in macrophages (Samavati et al., 2009). In cancer cells, dimeric PKM2 can use PEP as a phosphate donor to phosphorylate tyrosine residues in STAT3 (Gao et al., 2012; Yang et al., 2014b, 2015). To explore STAT3's role in glycolysis-driven and ROS-induced maldifferentiation, we assessed

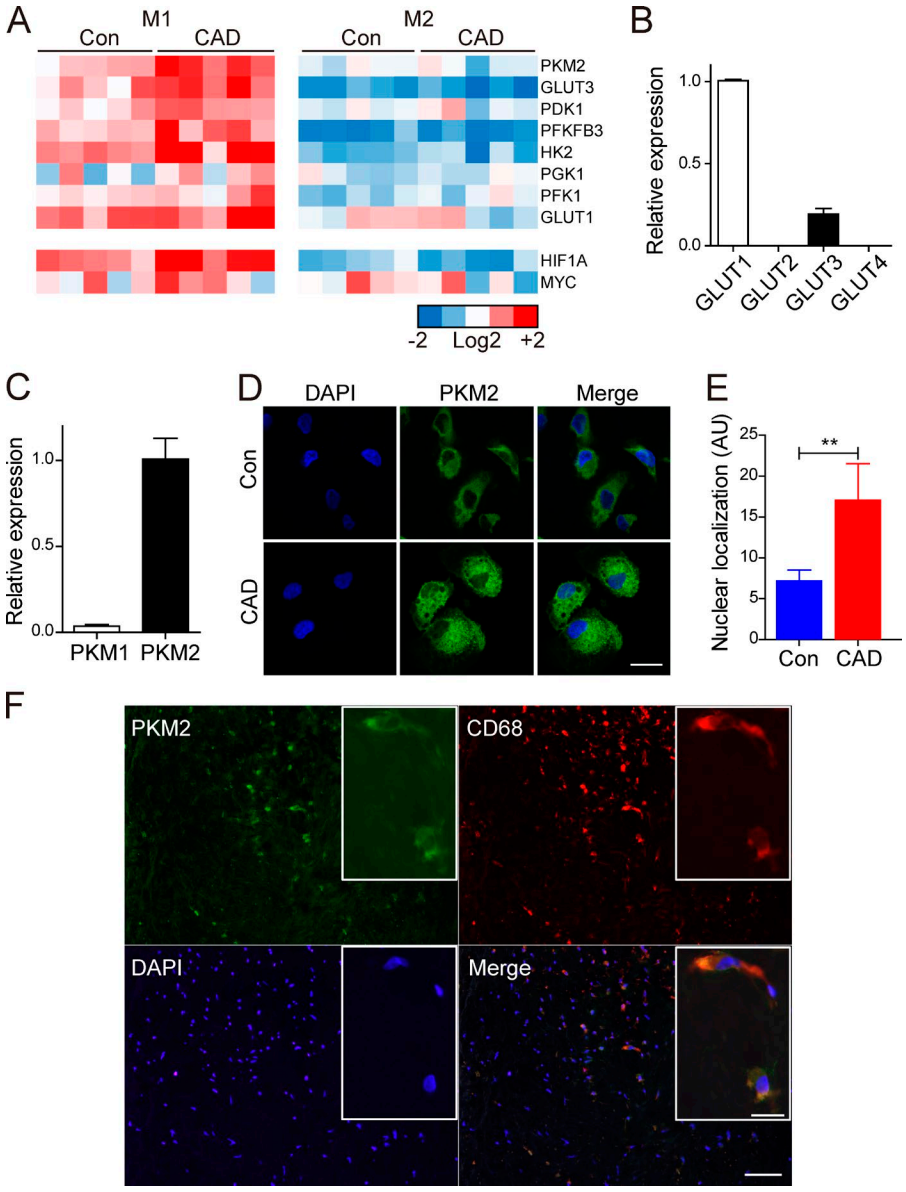

Figure 7. **Overexpression of the glycolytic enzyme PKM2 in CAD macrophages.** (A) Ex vivo–generated macrophages from five controls and five CAD patients were stimulated with LPS/IFN-γ (M1) or IL-4/IL-13 (M2) for 48 h and genes related to glucose metabolism were quantified by RT-PCR. Heat map displays the fold change increase of gene expression presented as the $\log_2$ value of relative mRNA expression (see color scale). (B) Total RNA was purified from macrophages, and expression of the glucose transporters GLUT1-4 was measured by qRT-PCR (n = 3). (C) Gene expression of the PKM1 and PKM2 isoforms in CAD macrophages was assessed by RT-PCR in three independent experiments. (D) Confocal images were acquired in ex vivo–generated macrophages stimulated with LPS/IFN-γ for 3 h and stained with anti-PKM2 (green). Nuclei were localized by DAPI (blue). Bars, 20 µm. (E) Bar graph represents averaged data from experiments quantifying the fluorescent signal within nuclei (n = 4 healthy controls and n = 7 CAD patients). All data are mean ± SEM. **, $P < 0.01$. (F) Frozen sections of carotid atheromas were stained with anti-PKM2 (green), anti-CD68 (red), and DAPI (blue) and analyzed by fluorescence microscopy. One representative of four independent experiments is shown. Bars, 100 µm; (inset) 20 µm.

STAT3 phosphorylation under M1-polarizing conditions. M1 stimulation clearly induced phosphorylation of STAT3 at Y705 (Fig. 9 B), and treatment with a STAT3-specific phosphorylation inhibitor, Stattic (McMurray, 2006), significantly reduced IL-6 and IL-1β (Fig. 9, C and D). Removal of ROS or restriction of glycolytic breakdown effectively interfered with pSTAT3 accumulation (Fig. 9, E–G), verifying the role of ROS and glucose metabolism in STAT3 activation.

To test whether PKM2 dimerization affected STAT3 phosphorylation, we forced PKM2 into tetrameric assembly with ML265. Preventing PKM2 dimerization reduced STAT3 phosphorylation (Fig. 9, H and I). To visualize the physical association of PKM2 and pSTAT3, we used the proximity ligation assay (PLA). In resting M0 cells, PKM2 and pSTAT3 did not co-localize, but came together exclusively in the nucleus after LPS/IFN-γ stimulation (Fig. 9 J). ROS scavenging (Tempol), slowing glycolysis (2-DG), and preventing PKM2 dimer formation (ML265) were all highly effective in preventing nuclear PKM2-pSTAT3 co-localization (Fig. 9 K).

DISCUSSION

Macrophages are key pathogenic drivers of vascular disease; they produce inflammatory cytokines, inflammation-accelerating chemokines, tissue-damaging proteases, and ROS. The current study demonstrates that monocytes and macrophages from CAD patients maldifferentiate and respond to M1-polarizing conditions with a hyperinflammatory phenotype. Gene expression studies (Fig. 2 A) identified a signature consisting of a cluster of cytokines and oxidative stress markers, which predicted that these innate immune cells are unable

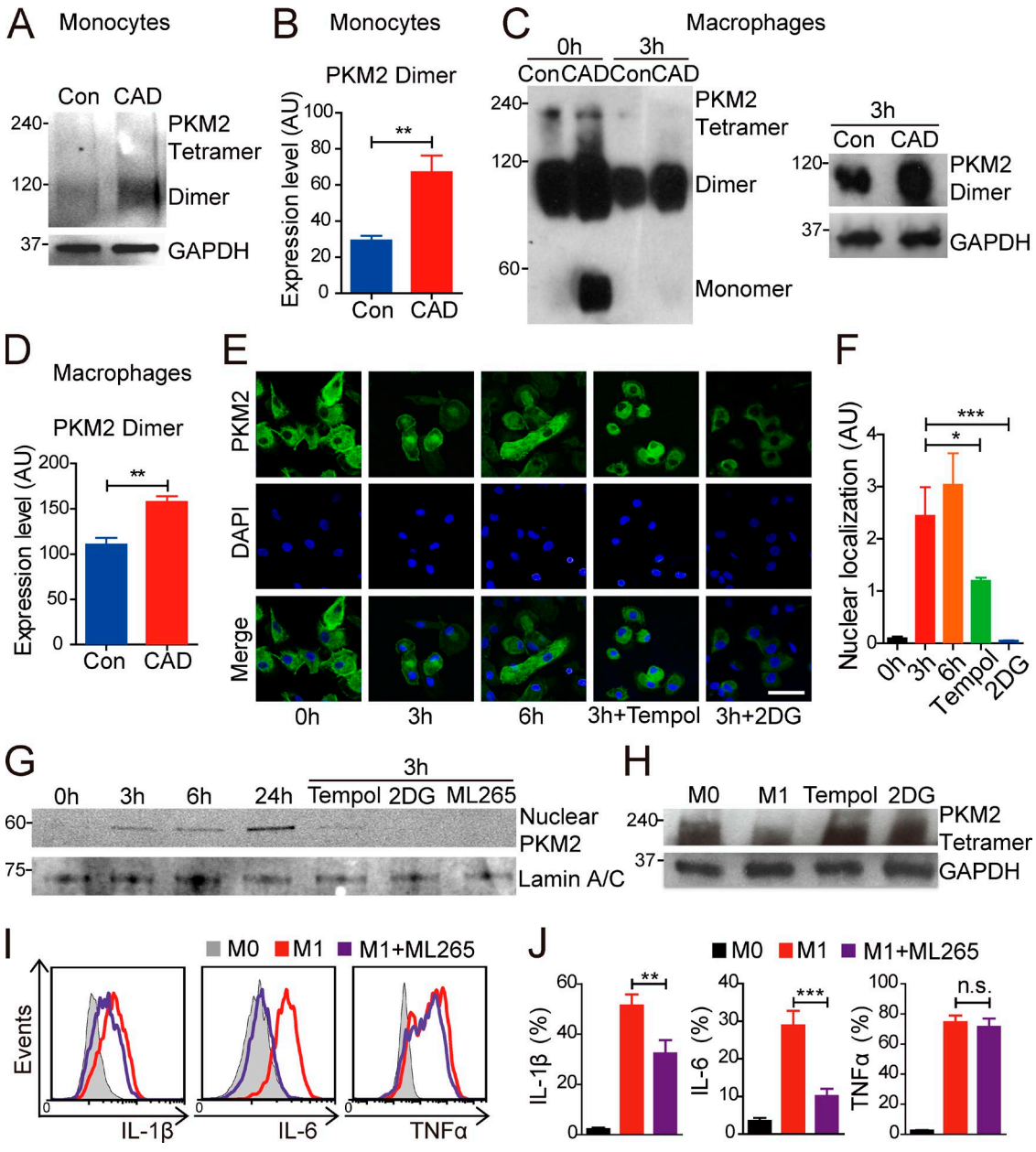

Figure 8. **Dimeric PKM2 in inflammatory CAD monocytes and macrophages.** (A) Monocytes from healthy controls and CAD patients were activated with LPS/IFN-γ. Cells were treated with 5 mM of di-succinimidyl suberate for 30 min before lysis, and protein extracts were analyzed by immunoblotting to identify oligomeric forms of PKM2. (B) Bar graph represents averaged data from $n = 8$ healthy controls and $n = 9$ CAD patients. (C) Macrophages from healthy controls and CAD patients were stimulated with LPS/IFN-γ, and protein extracts were analyzed by immunoblotting to identify oligomeric forms of PKM2. GAPDH was used as a loading control. (D) Bar graph represents averaged immunoblot data from seven independent experiments. (E) CAD macrophages were stained with anti-PKM2 (green) as indicated. Aliquots were treated with Tempol (50 µM) or 2-DG (10 mM). Distribution of PKM2 was analyzed by confocal microscopy. Nuclei were localized by DAPI (blue). Bar, 50 µm. (F) The bar graphs represent averaged data of the fluorescent signal within the nucleus ($n = 5–6$). (G) Nuclear protein extracts from CAD macrophages were analyzed by immunoblotting to identify PKM2. Lamin A/C was used as loading control. One representative of two independent experiments is shown. (H) Tetrameric assemblies of PKM2 were resolved by immunoblotting protein extracts of CAD macrophages prepared under nonreducing conditions. Aliquots were stimulated in the presence of Tempol or 2-DG. One representative of three independent experiments is shown. (I and J) PKM2 dimerization was inhibited in CAD macrophages by treating with ML265 (50 µM). Intracellular cytokines were measured by flow cytometry. Representative histograms (I) and summary of 8 independent experiments (J) are shown. Values are mean ± SEM. *, $P < 0.05$; **, $P < 0.01$; ***, $P < 0.001$.

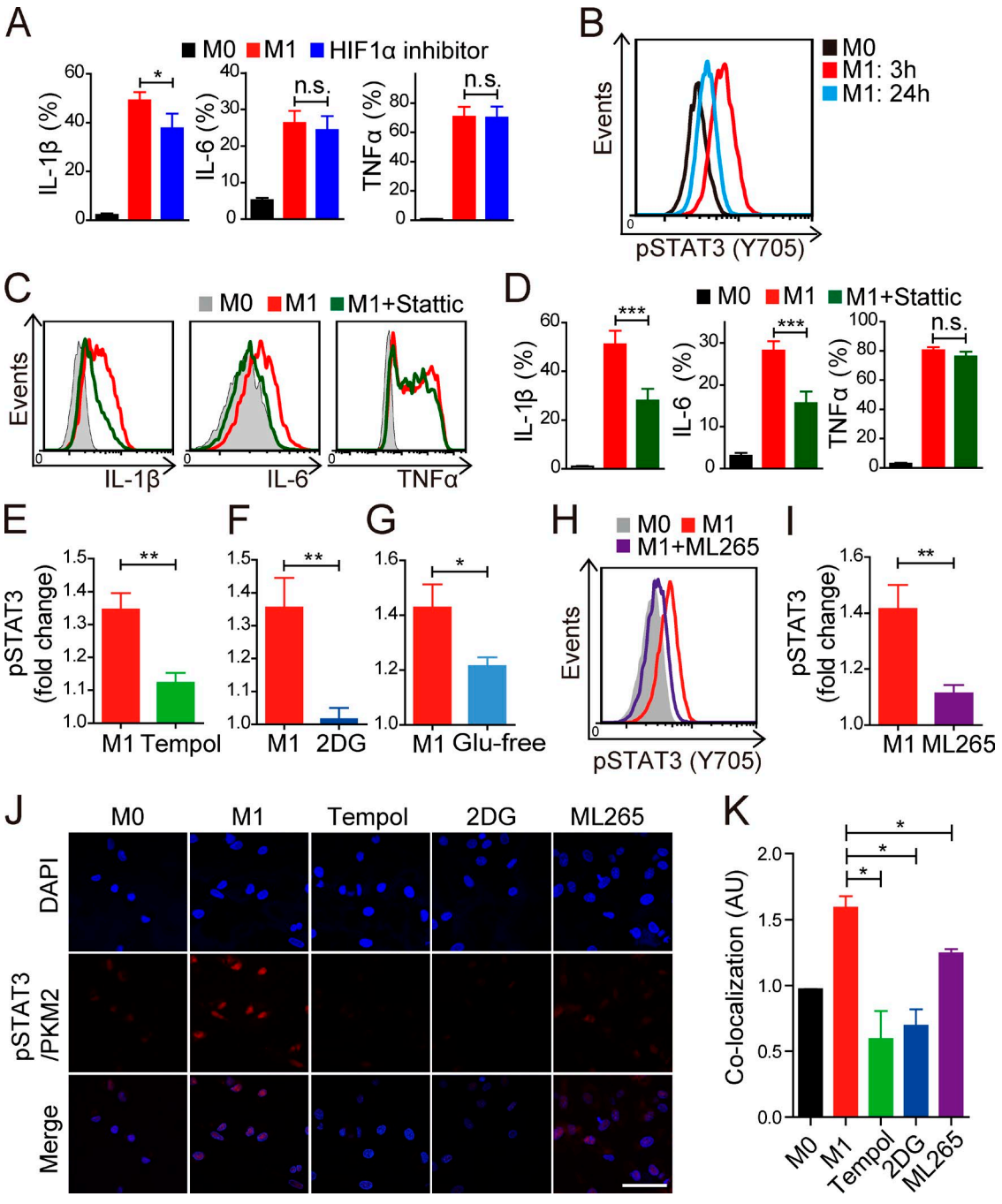

Figure 9. **PKM2 regulates inflammatory effector functions via phosphorylation of STAT3.** (A) CAD macrophages were stimulated for 6 h with or without the HIF-1α inhibitor CAS 934593-90-5 (10 µM). Intracellular cytokines were measured by flow cytometry in $n = 5$ experiments. (B) CAD macrophages were stimulated for 0, 3, and 24 h, and phosphorylation of STAT3 (Y705) was analyzed by flow cytometry. One representative of 3 independent experiments is shown. (C and D) CAD macrophages were stimulated for 6 h with or without the STAT3 inhibitor Stattic (5 µM) and intracellular cytokines were measured by flow cytometry. Representative histograms and results from 7 independent experiments are shown. (E–G) pSTAT3 was quantified by flow cytometry in CAD macrophages 3 h after stimulation in the absence or presence of Tempol (E; $n = 5$), 2-DG (F; $n = 5$), or glucose-free medium (G; $n = 6$). The fold change in MFI is plotted. (H and I) CAD macrophages were treated with ML265, stimulated and analyzed for pSTAT3 by flow cytometry. Representative histograms and results from 5 independent experiments. (J) Co-localization of pSTAT3 and PKM2 analyzed by confocal microscopy. Resting (M0) or M1-stimulated CAD macrophages in the absence (M1) and presence of Tempol, 2-DG, or ML265, were stained with anti-pSTAT3 and anti-PKM2. Close proximity (<40 nm) of pSTAT3 and PKM2 produces a red fluorescent signal. The blue signal indicates DAPI-stained nuclei. Bar, 50 µm. (K) Quantification of the fluorescent signal produced by pSTAT3/PKM2 co-localization ($n = 4$). Values represent mean ± SEM. *, $P < 0.05$; **, $P < 0.01$; ***, $P < 0.001$.

to properly detoxify ROS. Both patient-derived monocytes and macrophages produce excessive amounts of IL-6 and IL-1β. Circulating monocyte populations in CAD patients were characterized by a more than threefold expansion of the $CD14^{++}CD16^{+}$ intermediate population, which was poised for IL-6 and IL-1β production, and the abnormality persisted as the cells matured into macrophages, consistent with a defect that affects monocytic cells relatively early in their life cycle. Molecular studies implicated the glucose–ROS–PKM2–STAT3 pathway, in which glucose overutilization leads to unbalanced ROS generation (Fig. 5 I) and the redox-sensitive enzyme PKM2 transitions from the cytoplasm into the nucleus (Fig. 8, E–G). Nuclear PKM2 functions as a protein kinase, activates STAT3, and drives IL-6 and IL-1β transcription in a pSTAT3-dependent manner (Fig. 9, C, D, and H–K). Thus, hyperinflammatory macrophage reactivity is rooted in nutrient oversupply, compatible with gene-environment interactions that ultimately lead to host-damaging immune responses. This study identifies a new paradigm in human atherosclerosis, where PKM2 acts as a master regulator and the glucose–ROS–PKM2–STAT3 axis provides entirely new opportunities for antiinflammatory interventions in cardiovascular disease.

Individuals with diabetes or with prediabetic metabolic abnormalities are at high risk for aggressive atherosclerotic disease (Selvin et al., 2004). Glycemic control is recognized as effective in preventing microvascular complications (Fox et al., 2015). The benefit of reducing blood glucose levels for prevention of macrovascular disease is more nuanced, with an overall modest but statistically significant reduction in major cardiovascular disease outcomes (Ray et al., 2009; Boussageon et al., 2011). Here, we provide a molecular framework connecting glucose overutilization to deleterious inflammatory effector functions committed by monocytes and macrophages. In tissue studies, we found that atheroma-residing macrophages almost all express high levels of PKM2 (Fig. 7 F). CAD macrophages had a signature of parallel activation of glucose transporters and genes mediating glycolytic breakdown (Fig. 7 A). Remarkably, pyruvate dehydrogenase kinase was part of the transcriptional program, signifying a decoupling of glycolysis from the glutamine-fueled TCA cycle and essentially removing CAD macrophages from physiological control mechanisms. We further demonstrated that 2-DG, which starves cells of glucose, is a highly effective intervention to normalize CAD macrophage cytokine production (Fig. 5, A and B). ROS scavenging and enforcing PKM2 tetramerization were partially successful, suggesting that the pinnacle abnormality lies in glucose oversupply of the cells. Indeed, even resting monocytes and macrophages of CAD patients over-use glucose (Fig. 5, G and H), strongly supporting the notion that excess availability of glucose is a fundamental defect. Glucose utilization fueling cytokine production was selective for IL-6 and IL-1β, and excluded TNF, in line with a lack of clinical benefit from TNF blockade in CAD patients. Interference with glycolysis and ROS production left TNF unaffected, indicative of separate regulatory networks for the proinflammatory cytokines. Notably, TNF behaved differently from IL-6 and IL-1β, in that TNF production was higher in CAD monocytes, but indistinguishable in macrophages from cases and controls.

A second defect in CAD macrophages lies in the breakdown of PKM2-controlled negative feedback mechanisms. PKM2 exerts check point control of cellular energy levels, redox homeostasis, production of secretable biomass and cellular proliferation. To integrate these functions, the enzyme has pleotropic capabilities and, in CAD macrophages, several of its functional activities are critically involved in converting host-protective immune cells into injurious effector cells. Physiologically, PKM2 hyperactivity is disrupted by negative feedback regulation, readapting the cell's glycolytic activity to its needs. Our current data indicate that this mechanism is malfunctioning in CAD macrophages. Normally, posttranslational PKM2 modifications shift the equilibrium between high-activity tetramers and low-activity dimers. PKM2 phosphorylation at Y105 inhibits tetramer formation by causing the release of fructose 1,6-bisphosphate (Christofk et al., 2008b; Hitosugi et al., 2009). High glucose concentration stimulates PKM2 acetylation, which decreases enzyme activity, promotes lysosomal-dependent degradation via chaperone-mediated autophagy (Lv et al., 2011), and leads to nuclear loading with monomeric and dimeric PKM2 (Lv et al., 2013). Intracellular ROS oxidize PKM2 at C358 (Anastasiou et al., 2011). Succinyl-5-aminoimidazole-4-carboxamide-1-ribose-5′-phosphate binding induces nuclear import and protein kinase activity of PKM2 (Keller et al., 2014). In human monocytes and macrophages, the major oligomeric status of PKM2 is the dimer (Fig. 8, A and C), which is different from the dominance of monomers in mouse cells (Palsson-McDermott et al., 2015) and suggests species-specific regulatory mechanisms. In human macrophages, monomers and tetramers disappear and PKM2 transitions into the nucleus after stimulation (Fig. 8, C and E–G). Inhibition of glycolysis by 2-DG and scavenging ROS by Tempol suppress these changes, implying that oxidation-dependent PKM2 modification is necessary for its nuclear import. Given that dimeric PKM2 appears to be the dominant form of PKM2 in human macrophages, it is unlikely that dimerization alone is sufficient to enable nuclear import. Further studies need to explore why negative feedback mechanisms seem to fail in CAD cells, permitting glycolysis to progress unopposed. One possibility is that dimeric PKM2 acts in a positive feed-forward loop, enhancing the glycolytic machinery by bolstering c-Myc and HIF-1α. Also, PKM2 dimerization, by funneling glucose into the pentose phosphate pathways, enhances availability of biosynthetic precursor molecules required for cytokine synthesis. In essence, PKM2 dimerization directly and indirectly feeds the pathogenic behavior of inflammatory macrophages (Yang et al., 2014a).

One remarkable finding of the current study was the persistence of differences in metabolic and cytokine regu-

lation from monocytes to ex vivo–matured macrophages, compatible with patient-specific differences in epigenetic imprinting. Macrophages clearly memorized the metabolic reprogramming of their precursor cells. Recent data show that monocytes can build immunological memory via epigenetic reprogramming, and epigenetic pathways are now considered as potential therapeutic targets in atherosclerosis (Neele et al., 2015). Exposure of monocytes to oxidized low-density lipoprotein induces histone modifications that result in a long-lasting proinflammatory phenotype (Bekkering et al., 2014). Also, smoking, one of the strongest risk factors for CAD, is associated with DNA methylation (Reynolds et al., 2015). Notably, PKM2 is required for dissociation of histone deacetylase 3 from the Myc promoter (Yang et al., 2012), which implies a role in epigenetic regulation of macrophage polarization (Ivashkiv, 2013).

The unexpected finding of this study was the critical role of ROS in regulating cytokine production and, more importantly, that ROS were derived from the mitochondria and not from NOX2, a quintessential ROS source in phagocytic cells (Fig. 4, H and I). This does not discount the role of NOX2 in other pathological conditions. Indeed, we have recently shown a critical role of this subunit in immune activation of myeloid-derived dendritic cells, where it seems critical in lipid oxidation and formation of immunogenic isoketal-protein adducts (Kirabo et al., 2014; Wu et al., 2015). There is also evidence of substantial interplay between the NOX and mtROS production, such that one can enhance the other in a feed-forward fashion.

The coexistence of high glycolytic flux and PKM2 dimerization and the inability of the cells to rebalance their redox homeostasis suggest additional defects, possibly connected to control of mitochondrial function or perturbations of ROS scavenging. Decreased formation of metabolically active PKM2 should divert glucose into the pentose phosphate pathway and provide reducing potential to detoxify ROS. In CAD macrophages, even chronically elevated ROS concentrations are insufficient to disrupt further glycolytic flux. Also, the elevation of intracellular ROS in nonstimulated cells emphasizes that the redox balance is fundamentally flawed.

Scavenging mtROS had antiinflammatory effects and glucose feeding directly induced mtROS formation. Overexpression of the GLUT1 enhances ROS production in RAW264.7 macrophages, identifying glucose supply as a critical factor in setting mitochondrial activity (Freemerman et al., 2014). Recent studies have molecularly connected oxidative stress and proinflammatory cytokine production with mtROS functioning as signal-transducing molecules that up-regulate inflammatory cytokines via distinct molecular pathways (Naik and Dixit, 2011; Jin et al., 2014; Wang et al., 2014). Elevated mtROS levels correlate with persistent activation of JNK and p38 in periodic fever syndromes (Bulua et al., 2011). Also, divergent inflammasome-dependent pathways have been implicated in cytokine production regulated by mitochondrial dysfunction (Nakahira et al., 2011; Zhou et al., 2011). Analysis of mitochondrial respiration and of extramitochondrial glycolysis revealed a robust up-regulation of both energy-generating pathways in patient-derived cells. The defect was present in monocytes and maintained in macrophages. Although the poststimulation enhancement of glycolytic flux was expected, the persistently high oxygen consumption in patient-derived cells was indicative of continuously high mitochondrial activity and a failure to properly balance extramitochondrial and mitochondrial energy production. Further evidence for mitochondrial dysfunction came from uncoupling experiments, which revealed a robust respiratory reserve capacity in patient-derived cells. Insufficient uncoupling is a primary mechanism driving mtROS production and essentially indicates that mitochondria in CAD cells have lost a major protective mechanism. Possible causes include chronic glucose overload, in line with the surplus glucose uptake shown in Fig. 5 and the up-regulation of glucose transporters shown in Fig. 7. The defect was present in nondiabetic patients, eliminating elevated blood glucose as the sole cause. Persistent up-regulation of the glucose transporters and the glycolytic machinery suggest a fundamental abnormality in glucose handling. Also, molecular studies are needed to explore the underlying defects that allow the cells to tightly couple respiration with ATP generation and weaken physiological protection mechanisms. To date, molecular evidence for mitochondrial damage in CAD monocytes and macrophages is lacking.

Direct proinflammatory effects of glucose are difficult to distinguish from general energy needs that immune cells have; the distinction will require direct and detailed comparisons of healthy and patient-derived cells. Glycolytic activity supports de novo synthesis of fatty acids in dendritic cells, 2-DG reduces protein synthesis because of insufficient ER/Golgi formation, and glycolysis alters the posttranslational regulation of IL-6, IL-12, and TNF (Everts et al., 2014). In CAD macrophages, both Tempol and 2-DG suppressed, but did not abrogate IL-6 and IL-1β transcription, suggesting that ROS/glucose-dependent cytokine production can be therapeutically targeted without threatening the cell's survival. Tannahill et al. (2013) have implicated a succinate-dependent mechanism in regulating IL-1β, but not IL-6 or TNF production through a direct stabilizing effect of succinate on HIF-1α, which in turn functions as a transcriptional coactivator specifically for IL-1β, but not IL-6. In contrast, macrophages from CAD patients maldifferentiate into IL-6 and IL-1β–producing effector cells (Fig. 2, E–G). In this pathology, IL-6 holds particular relevance, as it dovetails with epidemiological studies identifying IL-6 as a robust biomarker for cardiovascular risk (Ridker et al., 2000). IL-6 also provides important signals to T cells, driving them from the antiinflammatory T regulatory phenotype to IL-17–producing cells (Korn et al., 2008). In human atherosclerosis, IL-6 appears to hold a pinnacle role among other proinflammatory cytokines.

A limitation of the current study is the use of human samples, donated by healthy individuals and patients. Al-

though we rigorously matched for age and sample handling, we did not match for medications or for diet. The persistence of the functional abnormalities in macrophages during ex vivo culture made an acute drug effect unlikely. To further examine whether drugs used in CAD management could prime monocytes to develop into proinflammatory macrophages, we studied cells from healthy individuals, who were taking such medications (aspirin, statins, β-blockers, and ACE inhibitors; Fig. 2 H) and did not observe an impact on cytokine production. Also, such medications have been considered to have antiinflammatory, and not proinflammatory, effects.

Our study has potential implications for the treatment of CAD and its associated inflammation. Interventions targeting lipids reduce acute coronary events, but have marginal effects on atheroma volume (Libby, 2013). Lipid-lowering therapies may confer plaque stabilization, trumping mechanical interventions that reduce luminal stenosis without modifying plaque inflammation (Libby and Aikawa, 2002). Because patients appropriately treated with statins are still at considerable risk for CAD, there is great unmet need for novel therapeutic strategies. Anti-inflammatory approaches are being explored for prevention of acute coronary syndrome (Everett et al., 2013). The Canakinumab Antiinflammatory Thrombosis Outcomes Study is assessing IL-1β inhibition in CAD (Ridker et al., 2011). Possibly, normalization of IL-1β and IL-6 production in macrophages would be even more effective without imposing broad immunosuppression on the host. The NIH has launched a trial to evaluate the use of the broad immunosuppressant methotrexate for preventing cardiovascular events. Targeting the glucose–ROS–PKM2–STAT3 pathway would allow suppressing not only excessive IL-1β, but also preventing overproduction of IL-6, thus correcting the hyperinflammatory behavior of the innate immune system in atherosclerotic patients. Because TNF is spared from this pathomechanism, this important immune defense would remain intact. A core abnormality of CAD monocytic cells lies in their excess ROS production, which is surprisingly NOX independent. A better understanding of that defect should allow the design of upstream interventions. In malignant cells, PKM2 is a key mediator of the Warburg effect, fueling cancer cell growth through metabolic rewiring. Similarities in the molecular reprogramming of cancer cells and CAD macrophages should be therapeutically exploited, and medications with anti-Warburg effects could be repurposed to treat cardiovascular disease.

MATERIALS AND METHODS

Patients and controls. The study population included 140 CAD patients and 105 healthy control subjects. Patients had unequivocal CAD with at least one documented myocardial infarction and were enrolled >90 d after an ischemic event. Demographic characteristics of the patients are given in Table 1. Demographically matched healthy individuals were recruited from the Stanford Blood Center (n = 105; age: 66.8 ± 7.1 yr; 90.5% male). They had no personal or family history of autoimmune disease, cancer, chronic viral infection, or any other inflammatory syndrome. The study was approved by the Institutional Review Board and written informed consent was obtained from all participants.

Table 1. **Clinical characteristics of patients with CAD**

Parameters	Patients (n = 140)
Age (mean ± SD)	70.0 ± 8.4
Male	99.0%
Ethnicity	
Caucasian	76.6%
African-American	3.7%
Asian	9.3%
BMI (mean ± SD)	30.9 ± 5.7
Diabetes mellitus	53.1%
Hypertension	85.7%
Hyperlipidemia	88.0%
Family history of CAD	32.4%
Smoking	
Current	12.5%
Former	73.7%
Treatment	
ACE inhibitor	48.6%
ATII receptor blocker	28.6%
β-blocker	76.4%
Ca-antagonist	44.4%
Diuretic	38.0%
Anti-platelet	81.1%
Anti-coagulant	30.6%
Statin	90.5%
Biguanide	23.9%
Sulfonylurea	10.3%
Insulin	20.6%

Cells and culture. PBMCs were isolated using density gradient centrifugation using Lymphoprep (STEMCELL Technologies). Monocytes isolated by plastic adherence were differentiated into macrophages in RPMI 1640 medium (Life Technologies) supplemented with 20 ng/ml of M-CSF (eBioscience) and 10% of FBS (Lonza) for 5 d. Alternatively, monocytes were isolated using the EasySep human monocyte enrichment kit without CD16 depletion (STEMCE LL Technologies). Macrophages were further differentiated into M1 or M2 macrophages by stimulation with 100 U/ml of IFN-γ (Sino Biologicals) and 100 ng/ml of LPS (Sigma-Aldrich), or 10 ng/ml of IL-4 and 10 ng/ml of IL-13 (Sino Biologicals). Attached macrophages were dissociated from plates using StemPro Accutase Cell Dissociation Reagent (Life Technologies).

To scavenge ROS, macrophages were stimulated in the presence of the ROS-scavenger Tempol (Sigma-Aldrich) or the mtROS scavenger MitoTempo (Santa Cruz Biotechnology, Inc.). Assembly of the NOX2 membrane complex was inhibited with gp91dstat (Anaspec). Glycolytic activity was blocked with 10 mM of 2-DG or by using glucose free RPMI 1640 medium (Life Technologies). PKM2 tetramerization

was enforced with 50 μM of ML265 (Cayman Chemical). HIF-1α was inhibited with 10 μM of CAS (934593–90-5; Santa Cruz Biotechnology, Inc.). STAT3 phosphorylation was inhibited with 5 μM of Stattic (Sigma-Aldrich).

Quantitative RT-PCR. Total RNA was extracted with RNeasy Mini kits (QIAGEN) and cDNA was reverse transcribed using a Maxima First Strand cDNA Synthesis Kit (Thermo Fisher Scientific). The expression of genes was determined using QuantiTect SYBR Green PCR master mix (Thermo Fisher Scientific) and a Real Plex2 Mastercycler (Eppendorf). The primers used are listed in Table S1. Gene transcript numbers were standardized and adjusted relative to β-actin transcripts.

Flow cytometry. CD14 and CD16 surface expression was measured using the FACS Fortessa (BD); data were analyzed with FlowJo Software (Tree Star). Monocyte subpopulations were sorted with the FACSAria II (BD). Monocytes were stained with allophycocyanin (APC)-conjugated anti-CD14 (BD), Pacific Blue–conjugated anti-CD16 (BioLegend), and FITC-conjugated anti–HLA-DR (BD). To evaluate cytokine production in macrophages, intracellular cytokine staining was performed in resting and stimulated cells (LPS and IFN-γ for the indicated hours). Golgi stop (BD) was added for the last 6 h of culture. Macrophages were stained with APC-conjugated anti-CD14 antibodies (BD), permeabilized using the Cytofix/Cytoperm Kit (BD), and stained with Pacific Blue–conjugated anti–IL-1β antibodies (BioLegend), FITC-conjugated anti–IL-6 antibodies (BioLegend), and phycoerythrin-conjugated anti-TNF antibodies (BD). Cell viability was assessed by 7-amino-actinomycin D (BD) staining.

Measurement of ROS. Macrophages or monocytes were stimulated with LPS and IFN-γ for the indicated times in RPMI medium with the indicated glucose concentrations, and then stained with 5 μM of CellROX Deep Red reagent (Molecular Probes) for 30 min or MitoSOX (Molecular Probes) for 10 min at 37°C. Macrophages were then washed with PBS and analyzed by flow cytometry.

Measurement of glucose uptake. Resting or stimulated macrophages or monocytes were incubated in glucose-free RPMI medium containing 5 μM of fluorescent d-glucose analogue 2-[N-(7-nitrobenz-2-oxa-1,3-diazol-4-yl) amino]-2-deoxy-d-glucose (Cayman Chemical) for 60 min at 37°C (Zou et al., 2005). Fluorescent intensities were analyzed by flow cytometry.

siRNA-mediated knockdown. To knock down NOX2 expression, 1 nM of small interference RNA oligonucleotides were transfected into macrophages using INTERFERin (Polyplus Transfection). Oligo duplex RNA specific for NOX2 was purchased from Life Technologies. As a negative control, negative control siRNA (Life Technologies) was used. 48 h after transfection, macrophages were stimulated as described in Cells and culture.

Mitochondrial respiration and glycolysis assays. Cellular OCR and ECAR were measured in monocytes and macrophages stimulated with LPS and INF-γ for 3 h. Measurements were taken at 37°C using an XF96 extracellular analyzer (Seahorse Bioscience). Cells were seeded in 96-well plates and medium was changed to unbuffered DMEM (DMEM supplemented with 25 mM glucose, 31 mM NaCl, and 2 mM GlutaMax, pH 7.4) and incubated at 37°C in a non-CO_2 incubator for 1 h. All reagents were adjusted to pH 7.4. Three measurements were taken before and after addition of oligomycin (1 μg/ml), FCCP (0.5 μM), and the combination of antimycin A (10 μM) and rotenone (10 μM). OCR and ECAR were calculated by the Seahorse Wave software.

Western blotting. Monocytes and macrophages were collected and lysed in lysis buffer (50 mM Hepes, pH 7.4, 50 mM, NaCl, 1% Triton X-100, 5 mM EDTA, 1 mM PMSF, 10 g/ml aprotinin, 10 g/ml leupeptin, 10 mM sodium pyrophosphate, 50 mM sodium fluoride, and 1 mM sodium orthovanadate). Nuclear proteins were extracted using NE-PER Nuclear and Cytoplasmic Extraction Reagents (Thermo Fisher Scientific). Nonreducing conditions were applied for the detection of PKM2 dimeric and tetrameric forms. For the detection of oligomers, cells were treated with 5 mM of di-succinimidyl suberate (Thermo Fisher Scientific) for 30 min before lysis. Lysates were separated by SDS-PAGE, transferred to nitrocellulose membranes, and incubated with the following antibodies: anti-PKM2 (Cell Signaling Technology), anti-GAPDH (Santa Cruz Biotechnology, Inc.), anti-Lamin A/C (Genentech), horseradish peroxidase-conjugated anti-Ig (Santa Cruz Biotechnology, Inc.), and IRDye 800CW anti-Ig (LI-COR Biosciences). The enhanced chemiluminescence detection system (GE Healthcare) was used to detect bands with peroxidase activity, or membranes were scanned with an Odyssey fluorescence scanner (LI-COR).

Confocal microscopy. Differentiated and stimulated macrophages seeded on glass coverslips were incubated with specific antibodies for 1 h at room temperature, followed by Alexa Fluor 488–conjugated secondary antibodies (Life Technologies) for 1 h at room temperature. Cells on coverslips were mounted in Vectashield with DAPI (Vector Laboratories) and examined using the 488- and 405-nm lines of the argon ion and diode lasers in a confocal imaging system (LSM 710; Carl Zeiss). All experiments included controls without primary antibody.

Immunohistochemistry. OCT-embedded sections of carotid arteries from CAD patients were sectioned at 10-μm intervals and fixed with 4% paraformaldehyde solution (Affymetrix). After blocking with 5% normal goat serum (Invitrogen), sections were incubated with unconjugated primary antibody overnight. Primary antibodies included rabbit anti–human PKM2 (1:100; Cell Signaling Technology), rabbit anti-human IL-6 (1:400; Thermo Fisher Scientific) and mouse anti–

human CD68 (1:100; Dako). Isotype-matched primary antibodies served as control. Tissue sections were then stained with secondary antibodies, Alexa Fluor 488–conjugated goat anti–rabbit IgG and Alexa Fluor 544–conjugated goat anti–mouse IgG (Life Technologies) for 2 h, and mounted with DAPI-containing mounting medium (Molecular Probes). Tissue sections were examined using fluorescence microscopy.

Detection of STAT3 phosphorylation. Phosphorylation of STAT3 at Y705 was assessed at the single-cell level by Phosflow (BD). In brief, macrophages were stimulated with IFN-γ and LPS, fixed with Cytofix buffer (BD) at 37°C for 10 min, permeabilized with Phosflow Perm buffer III (BD) for 30 min on ice, and then stained with phycoerythrin-conjugated anti-pSTAT3 (Y705) antibodies (BD). Stained cells were analyzed by flow cytometry.

Proximity ligation assay (PLA). Resting and stimulated macrophages were attached to cover glasses; paraformaldehyde fixed and labeled with PKM2 or phospho-STAT3 (Y705) antibodies (Cell Signaling Technology). To visualize close co-localization of the two proteins, we applied the PLA protocol (Olink Bioscience), in which antibodies against a protein pair are attached to short chains of complementary DNA oligonucleotides, which hybridize when in close proximity. Enzymatic ligation of the oligonucleotides generates a circularized DNA strand that serves as a template. The amplification reaction product remains attached to the antibody-protein complex and is visualized through the hybridization of fluorescently labeled oligonucleotides. A fluorescence signal occurs only when two proteins are in close juxtaposition (40 nm). Signals of fluorescent PLA probes indicating co-localization/co-compartmentalization of two proteins were acquired with a confocal imaging system (LSM 710; Carl Zeiss).

Statistical analysis. Statistical significance was calculated by the Wilcoxon-Mann-Whitney test when comparing two groups or by one-way or two-way ANOVA when comparing three or more groups. All analyses were performed using Prism software (GraphPad Software). In all analyses, $P < 0.05$ was taken to indicate statistical significance. Power analysis was performed to minimally yield an 80% chance to detect a significant difference.

ACKNOWLEDGMENTS

This work was supported by grants from the National Institutes of Health (NIH; AR042547, AI044142, HL058000, AI108891, HL117913, AG045779) and by the Govenar Discovery Fund. R.R. Nazarewicz was supported in part by American Heart Association grant 14SDG20410081. The content is solely the responsibility of the authors and does not necessarily represent the official views of the NIH.

The authors declare no competing financial interests.

Submitted: 29 May 2015
Accepted: 1 February 2016

REFERENCES

Anastasiou, D., G. Poulogiannis, J.M. Asara, M.B. Boxer, J.K. Jiang, M. Shen, G. Bellinger, A.T. Sasaki, J.W. Locasale, D.S. Auld, et al. 2011. Inhibition of pyruvate kinase M2 by reactive oxygen species contributes to cellular antioxidant responses. *Science.* 334:1278–1283. http://dx.doi.org/10.1126/science.1211485

Bekkering, S., J. Quintin, L.A. Joosten, J.W. van der Meer, M.G. Netea, and N.P. Riksen. 2014. Oxidized low-density lipoprotein induces long-term proinflammatory cytokine production and foam cell formation via epigenetic reprogramming of monocytes. *Arterioscler. Thromb. Vasc. Biol.* 34:1731–1738. http://dx.doi.org/10.1161/ATVBAHA.114.303887

Boussageon, R., T. Bejan-Angoulvant, M. Saadatian-Elahi, S. Lafont, C. Bergeonneau, B. Kassaï, S. Erpeldinger, J.M. Wright, F. Gueyffier, and C. Cornu. 2011. Effect of intensive glucose lowering treatment on all cause mortality, cardiovascular death, and microvascular events in type 2 diabetes: meta-analysis of randomised controlled trials. *BMJ.* 343(jul26 1):d4169. http://dx.doi.org/10.1136/bmj.d4169

Bulua, A.C., A. Simon, R. Maddipati, M. Pelletier, H. Park, K.Y. Kim, M.N. Sack, D.L. Kastner, and R.M. Siegel. 2011. Mitochondrial reactive oxygen species promote production of proinflammatory cytokines and are elevated in TNFR1-associated periodic syndrome (TRAPS). *J. Exp. Med.* 208:519–533. http://dx.doi.org/10.1084/jem.20102049

Christofk, H.R., M.G. Vander Heiden, M.H. Harris, A. Ramanathan, R.E. Gerszten, R. Wei, M.D. Fleming, S.L. Schreiber, and L.C. Cantley. 2008a. The M2 splice isoform of pyruvate kinase is important for cancer metabolism and tumour growth. *Nature.* 452:230–233. http://dx.doi.org/10.1038/nature06734

Christofk, H.R., M.G. Vander Heiden, N. Wu, J.M. Asara, and L.C. Cantley. 2008b. Pyruvate kinase M2 is a phosphotyrosine-binding protein. *Nature.* 452:181–186. http://dx.doi.org/10.1038/nature06667

Colegio, O.R., N.Q. Chu, A.L. Szabo, T. Chu, A.M. Rhebergen, V. Jairam, N. Cyrus, C.E. Brokowski, S.C. Eisenbarth, G.M. Phillips, et al. 2014. Functional polarization of tumour-associated macrophages by tumour-derived lactic acid. *Nature.* 513:559–563. http://dx.doi.org/10.1038/nature13490

Dikalova, A.E., A.T. Bikineyeva, K. Budzyn, R.R. Nazarewicz, L. McCann, W. Lewis, D.G. Harrison, and S.I. Dikalov. 2010. Therapeutic targeting of mitochondrial superoxide in hypertension. *Circ. Res.* 107:106–116. http://dx.doi.org/10.1161/CIRCRESAHA.109.214601

Everett, B.M., A.D. Pradhan, D.H. Solomon, N. Paynter, J. Macfadyen, E. Zaharris, M. Gupta, M. Clearfield, P. Libby, A.A. Hasan, et al. 2013. Rationale and design of the Cardiovascular Inflammation Reduction Trial: a test of the inflammatory hypothesis of atherothrombosis. *Am. Heart J.* 166:199–207.e15. http://dx.doi.org/10.1016/j.ahj.2013.03.018

Everts, B., E. Amiel, S.C. Huang, A.M. Smith, C.H. Chang, W.Y. Lam, V. Redmann, T.C. Freitas, J. Blagih, G.J. van der Windt, et al. 2014. TLR-driven early glycolytic reprogramming via the kinases TBK1-IKKε supports the anabolic demands of dendritic cell activation. *Nat. Immunol.* 15:323–332. http://dx.doi.org/10.1038/ni.2833

Fearon, I.M., and S.P. Faux. 2009. Oxidative stress and cardiovascular disease: novel tools give (free) radical insight. *J. Mol. Cell. Cardiol.* 47:372–381. http://dx.doi.org/10.1016/j.yjmcc.2009.05.013

Fox, C.S., S.H. Golden, C. Anderson, G.A. Bray, L.E. Burke, I.H. de Boer, P. Deedwania, R.H. Eckel, A.G. Ershow, J. Fradkin, et al. American Heart Association Diabetes Committee of the Council on Lifestyle and Cardiometabolic Health, Council on Clinical Cardiology, Council on Cardiovascular and Stroke Nursing, Council on Cardiovascular Surgery and Anesthesia, Council on Quality of Care and Outcomes Research, and the American Diabetes Association. 2015. Update on Prevention of Cardiovascular Disease in Adults With Type 2 Diabetes Mellitus in Light of Recent Evidence: A Scientific Statement From the American Heart Association and the American Diabetes Association. *Circulation.* 132:691–718. http://dx.doi.org/10.1161/CIR.0000000000000230

Freemerman, A.J., A.R. Johnson, G.N. Sacks, J.J. Milner, E.L. Kirk, M.A. Troester, A.N. Macintyre, P. Goraksha-Hicks, J.C. Rathmell, and L. Makowski. 2014. Metabolic reprogramming of macrophages: glucose transporter 1 (GLUT1)-mediated glucose metabolism drives a proinflammatory phenotype. *J. Biol. Chem.* 289:7884–7896. http://dx.doi.org/10.1074/jbc.M113.522037

Gao, X., H. Wang, J.J. Yang, X. Liu, and Z.R. Liu. 2012. Pyruvate kinase M2 regulates gene transcription by acting as a protein kinase. *Mol. Cell.* 45:598–609. http://dx.doi.org/10.1016/j.molcel.2012.01.001

Grundy, S.M., H.B. Brewer Jr., J.I. Cleeman, S.C. Smith Jr., C. Lenfant American Heart Association. National Heart, Lung, and Blood Institute. 2004. Definition of metabolic syndrome: Report of the National Heart, Lung, and Blood Institute/American Heart Association conference on scientific issues related to definition. *Circulation.* 109:433–438. http://dx.doi.org/10.1161/01.CIR.0000111245.75752.C6

Hansson, G.K., and A. Hermansson. 2011. The immune system in atherosclerosis. *Nat. Immunol.* 12:204–212. http://dx.doi.org/10.1038/ni.2001

Hansson, G.K., and P. Libby. 2006. The immune response in atherosclerosis: a double-edged sword. *Nat. Rev. Immunol.* 6:508–519. http://dx.doi.org/10.1038/nri1882

Hitosugi, T., S. Kang, M.G. Vander Heiden, T.W. Chung, S. Elf, K. Lythgoe, S. Dong, S. Lonial, X. Wang, G.Z. Chen, et al. 2009. Tyrosine phosphorylation inhibits PKM2 to promote the Warburg effect and tumor growth. *Sci. Signal.* 2:ra73. http://dx.doi.org/10.1126/scisignal.2000431

Huang, S.C.C., and E.J. Pearce. 2014. For macrophages, Ndufs is enough. *Immunity.* 41:351–353. http://dx.doi.org/10.1016/j.immuni.2014.09.004

Itoh, K., J. Mimura, and M. Yamamoto. 2010. Discovery of the negative regulator of Nrf2, Keap1: a historical overview. *Antioxid. Redox Signal.* 13:1665–1678. http://dx.doi.org/10.1089/ars.2010.3222

Ivashkiv, L.B. 2013. Epigenetic regulation of macrophage polarization and function. *Trends Immunol.* 34:216–223. http://dx.doi.org/10.1016/j.it.2012.11.001

Jin, Z., W. Wei, M. Yang, Y. Du, and Y. Wan. 2014. Mitochondrial complex I activity suppresses inflammation and enhances bone resorption by shifting macrophage-osteoclast polarization. *Cell Metab.* 20:483–498. http://dx.doi.org/10.1016/j.cmet.2014.07.011

Keller, K.E., Z.M. Doctor, Z.W. Dwyer, and Y.S. Lee. 2014. SAICAR induces protein kinase activity of PKM2 that is necessary for sustained proliferative signaling of cancer cells. *Mol. Cell.* 53:700–709. http://dx.doi.org/10.1016/j.molcel.2014.02.015

Kirabo, A., V. Fontana, A.P. de Faria, R. Loperena, C.L. Galindo, J. Wu, A.T. Bikineyeva, S. Dikalov, L. Xiao, W. Chen, et al. 2014. DC isoketal-modified proteins activate T cells and promote hypertension. *J. Clin. Invest.* 124:4642–4656. http://dx.doi.org/10.1172/JCI74084

Korge, P., P. Ping, and J.N. Weiss. 2008. Reactive oxygen species production in energized cardiac mitochondria during hypoxia/reoxygenation: modulation by nitric oxide. *Circ. Res.* 103:873–880. http://dx.doi.org/10.1161/CIRCRESAHA.108.180869

Korn, T., M. Mitsdoerffer, A.L. Croxford, A. Awasthi, V.A. Dardalhon, G. Galileos, P. Vollmar, G.L. Stritesky, M.H. Kaplan, A. Waisman, et al. 2008. IL-6 controls Th17 immunity in vivo by inhibiting the conversion of conventional T cells into Foxp3+ regulatory T cells. *Proc. Natl. Acad. Sci. USA.* 105:18460–18465. http://dx.doi.org/10.1073/pnas.0809850105

Libby, P. 2013. Mechanisms of acute coronary syndromes and their implications for therapy. *N. Engl. J. Med.* 368:2004–2013. http://dx.doi.org/10.1056/NEJMra1216063

Libby, P., and M. Aikawa. 2002. Stabilization of atherosclerotic plaques: new mechanisms and clinical targets. *Nat. Med.* 8:1257–1262. http://dx.doi.org/10.1038/nm1102-1257

Liu, H., R. Colavitti, I.I. Rovira, and T. Finkel. 2005. Redox-dependent transcriptional regulation. *Circ. Res.* 97:967–974. http://dx.doi.org/10.1161/01.RES.0000188210.72062.10

Luo, W., H. Hu, R. Chang, J. Zhong, M. Knabel, R. O'Meally, R.N. Cole, A. Pandey, and G.L. Semenza. 2011. Pyruvate kinase M2 is a PHD3-stimulated coactivator for hypoxia-inducible factor 1. *Cell.* 145:732–744. http://dx.doi.org/10.1016/j.cell.2011.03.054

Lv, L., D. Li, D. Zhao, R. Lin, Y. Chu, H. Zhang, Z. Zha, Y. Liu, Z. Li, Y. Xu, et al. 2011. Acetylation targets the M2 isoform of pyruvate kinase for degradation through chaperone-mediated autophagy and promotes tumor growth. *Mol. Cell.* 42:719–730. http://dx.doi.org/10.1016/j.molcel.2011.04.025

Lv, L., Y.P. Xu, D. Zhao, F.L. Li, W. Wang, N. Sasaki, Y. Jiang, X. Zhou, T.T. Li, K.L. Guan, et al. 2013. Mitogenic and oncogenic stimulation of K433 acetylation promotes PKM2 protein kinase activity and nuclear localization. *Mol. Cell.* 52:340–352. http://dx.doi.org/10.1016/j.molcel.2013.09.004

Mahabeleshwar, G.H., D. Kawanami, N. Sharma, Y. Takami, G. Zhou, H. Shi, L. Nayak, D. Jeyaraj, R. Grealy, M. White, et al. 2011. The myeloid transcription factor KLF2 regulates the host response to polymicrobial infection and endotoxic shock. *Immunity.* 34:715–728. http://dx.doi.org/10.1016/j.immuni.2011.04.014

Martinez, F.O., and S. Gordon. 2014. The M1 and M2 paradigm of macrophage activation: time for reassessment. *F1000Prime Rep.* 6:13. http://dx.doi.org/10.12703/P6-13

Martinez, F.O., A. Sica, A. Mantovani, and M. Locati. 2008. Macrophage activation and polarization. *Front. Biosci.* 13:453–461. http://dx.doi.org/10.2741/2692

Martinez, F.O., L. Helming, R. Milde, A. Varin, B.N. Melgert, C. Draijer, B. Thomas, M. Fabbri, A. Crawshaw, L.P. Ho, et al. 2013. Genetic programs expressed in resting and IL-4 alternatively activated mouse and human macrophages: similarities and differences. *Blood.* 121:e57–e69. http://dx.doi.org/10.1182/blood-2012-06-436212

McMurray, J.S. 2006. A new small-molecule Stat3 inhibitor. *Chem. Biol.* 13:1123–1124. http://dx.doi.org/10.1016/j.chembiol.2006.11.001

Moore, K.J., F.J. Sheedy, and E.A. Fisher. 2013. Macrophages in atherosclerosis: a dynamic balance. *Nat. Rev. Immunol.* 13:709–721. http://dx.doi.org/10.1038/nri3520

Naik, E., and V.M. Dixit. 2011. Mitochondrial reactive oxygen species drive proinflammatory cytokine production. *J. Exp. Med.* 208:417–420. http://dx.doi.org/10.1084/jem.20110367

Nakahira, K., J.A. Haspel, V.A. Rathinam, S.J. Lee, T. Dolinay, H.C. Lam, J.A. Englert, M. Rabinovitch, M. Cernadas, H.P. Kim, et al. 2011. Autophagy proteins regulate innate immune responses by inhibiting the release of mitochondrial DNA mediated by the NALP3 inflammasome. *Nat. Immunol.* 12:222–230. http://dx.doi.org/10.1038/ni.1980

Nathan, C., and A. Cunningham-Bussel. 2013. Beyond oxidative stress: an immunologist's guide to reactive oxygen species. *Nat. Rev. Immunol.* 13:349–361. http://dx.doi.org/10.1038/nri3423

Neele, A.E., J. Van den Bossche, M.A. Hoeksema, and M.P.J. de Winther. 2015. Epigenetic pathways in macrophages emerge as novel targets in atherosclerosis. *Eur. J. Pharmacol.* 763(Pt A):79–89. http://dx.doi.org/10.1016/j.ejphar.2015.03.101

Noguchi, T., H. Inoue, and T. Tanaka. 1986. The M1- and M2-type isozymes of rat pyruvate kinase are produced from the same gene by alternative RNA splicing. *J. Biol. Chem.* 261:13807–13812.

O'Neill, L.A., and D.G. Hardie. 2013. Metabolism of inflammation limited by AMPK and pseudo-starvation. *Nature.* 493:346–355. http://dx.doi.org/10.1038/nature11862

Palsson-McDermott, E.M., A.M. Curtis, G. Goel, M.A. Lauterbach, F.J. Sheedy, L.E. Gleeson, M.W. van den Bosch, S.R. Quinn, R. Domingo-Fernandez, D.G. Johnston, et al. 2015. Pyruvate kinase M2 regulates

Hif-1α activity and IL-1β induction and is a critical determinant of the warburg effect in LPS-activated macrophages. *Cell Metab.* 21:65–80. http://dx.doi.org/10.1016/j.cmet.2014.12.005

Ralser, M., M.M. Wamelink, E.A. Struys, C. Joppich, S. Krobitsch, C. Jakobs, and H. Lehrach. 2008. A catabolic block does not sufficiently explain how 2-deoxy-D-glucose inhibits cell growth. *Proc. Natl. Acad. Sci. USA.* 105:17807–17811. http://dx.doi.org/10.1073/pnas.0803090105

Ray, K.K., S.R. Seshasai, S. Wijesuriya, R. Sivakumaran, S. Nethercott, D. Preiss, S. Erqou, and N. Sattar. 2009. Effect of intensive control of glucose on cardiovascular outcomes and death in patients with diabetes mellitus: a meta-analysis of randomised controlled trials. *Lancet.* 373:1765–1772. http://dx.doi.org/10.1016/S0140-6736(09)60697-8

Rey, F.E., M.E. Cifuentes, A. Kiarash, M.T. Quinn, and P.J. Pagano. 2001. Novel competitive inhibitor of NAD(P)H oxidase assembly attenuates vascular O(2)(-) and systolic blood pressure in mice. *Circ. Res.* 89:408–414. http://dx.doi.org/10.1161/hh1701.096037

Reynolds, L.M., M. Wan, J. Ding, J.R. Taylor, K. Lohman, D. Su, B.D. Bennett, D.K. Porter, R. Gimple, G.S. Pittman, et al. 2015. DNA Methylation of the Aryl Hydrocarbon Receptor Repressor Associations With Cigarette Smoking and Subclinical Atherosclerosis. *Circ Cardiovasc Genet.* 8:707–716. http://dx.doi.org/10.1161/CIRCGENETICS.115.001097

Ridker, P.M., N. Rifai, M.J. Stampfer, and C.H. Hennekens. 2000. Plasma concentration of interleukin-6 and the risk of future myocardial infarction among apparently healthy men. *Circulation.* 101:1767–1772. http://dx.doi.org/10.1161/01.CIR.101.15.1767

Ridker, P.M., E. Danielson, F.A. Fonseca, J. Genest, A.M. Gotto Jr., J.J. Kastelein, W. Koenig, P. Libby, A.J. Lorenzatti, J.G. MacFadyen, et al. JUPITER Study Group. 2008. Rosuvastatin to prevent vascular events in men and women with elevated C-reactive protein. *N. Engl. J. Med.* 359:2195–2207. http://dx.doi.org/10.1056/NEJMoa0807646

Ridker, P.M., T. Thuren, A. Zalewski, and P. Libby. 2011. Interleukin-1β inhibition and the prevention of recurrent cardiovascular events: rationale and design of the Canakinumab Anti-inflammatory Thrombosis Outcomes Study (CANTOS). *Am. Heart J.* 162:597–605. http://dx.doi.org/10.1016/j.ahj.2011.06.012

Rogacev, K.S., B. Cremers, A.M. Zawada, S. Seiler, N. Binder, P. Ege, G. Große-Dunker, I. Heisel, F. Hornof, J. Jeken, et al. 2012. CD14++CD16+ monocytes independently predict cardiovascular events: a cohort study of 951 patients referred for elective coronary angiography. *J. Am. Coll. Cardiol.* 60:1512–1520. http://dx.doi.org/10.1016/j.jacc.2012.07.019

Rudd, J.H., E.A. Warburton, T.D. Fryer, H.A. Jones, J.C. Clark, N. Antoun, P. Johnström, A.P. Davenport, P.J. Kirkpatrick, B.N. Arch, et al. 2002. Imaging atherosclerotic plaque inflammation with [18F]-fluorodeoxyglucose positron emission tomography. *Circulation.* 105:2708–2711. http://dx.doi.org/10.1161/01.CIR.0000020548.60110.76

Ruparelia, N., J. Godec, R. Lee, J.T. Chai, E. Dall'Armellina, D. McAndrew, J.E. Digby, J.C. Forfar, B.D. Prendergast, R.K. Kharbanda, et al. 2015. Acute myocardial infarction activates distinct inflammation and proliferation pathways in circulating monocytes, prior to recruitment, and identified through conserved transcriptional responses in mice and humans. *Eur. Heart J.* 36:1923–1934. http://dx.doi.org/10.1093/eurheartj/ehv195

Samavati, L., R. Rastogi, W. Du, M. Hüttemann, A. Fite, and L. Franchi. 2009. STAT3 tyrosine phosphorylation is critical for interleukin 1 beta and interleukin-6 production in response to lipopolysaccharide and live bacteria. *Mol. Immunol.* 46:1867–1877. http://dx.doi.org/10.1016/j.molimm.2009.02.018

Selvin, E., S. Marinopoulos, G. Berkenblit, T. Rami, F.L. Brancati, N.R. Powe, and S.H. Golden. 2004. Meta-analysis: glycosylated hemoglobin and cardiovascular disease in diabetes mellitus. *Ann. Intern. Med.* 141:421–431. http://dx.doi.org/10.7326/0003-4819-141-6-200409210-00007

Shirai, T., M. Hilhorst, D.G. Harrison, J.J. Goronzy, and C.M. Weyand. 2015. Macrophages in vascular inflammation—From atherosclerosis to vasculitis. *Autoimmunity.* 48:139–151. http://dx.doi.org/10.3109/08916934.2015.1027815

Stöger, J.L., M.J. Gijbels, S. van der Velden, M. Manca, C.M. van der Loos, E.A. Biessen, M.J. Daemen, E. Lutgens, and M.P. de Winther. 2012. Distribution of macrophage polarization markers in human atherosclerosis. *Atherosclerosis.* 225:461–468. http://dx.doi.org/10.1016/j.atherosclerosis.2012.09.013

Tannahill, G.M., A.M. Curtis, J. Adamik, E.M. Palsson-McDermott, A.F. McGettrick, G. Goel, C. Frezza, N.J. Bernard, B. Kelly, N.H. Foley, et al. 2013. Succinate is an inflammatory signal that induces IL-1β through HIF-1α. *Nature.* 496:238–242. http://dx.doi.org/10.1038/nature11986

Walsh, M.J., K.R. Brimacombe, D. Anastasiou, Y. Yu, W.J. Israelsen, B.S. Hong, W. Tempel, S. Dimov, H. Veith, H. Yang, et al. 2010. ML265: A potent PKM2 activator induces tetramerization and reduces tumor formation and size in a mouse xenograft model. *In* Probe Reports from the NIH Molecular Libraries Program. National Center for Biotechnology Information. Bethesda, MD.

Wang, Y., G.Z. Wang, P.S. Rabinovitch, and I. Tabas. 2014. Macrophage mitochondrial oxidative stress promotes atherosclerosis and nuclear factor-κB-mediated inflammation in macrophages. *Circ. Res.* 114:421–433. http://dx.doi.org/10.1161/CIRCRESAHA.114.302153

Wilcox, C.S. 2010. Effects of tempol and redox-cycling nitroxides in models of oxidative stress. *Pharmacol. Ther.* 126:119–145. http://dx.doi.org/10.1016/j.pharmthera.2010.01.003

Witztum, J.L., and A.H. Lichtman. 2014. The influence of innate and adaptive immune responses on atherosclerosis. *Annu. Rev. Pathol.* 9:73–102. http://dx.doi.org/10.1146/annurev-pathol-020712-163936

Wu, J., M.A. Saleh, A. Kirabo, H.A. Itani, K.R. Montaniel, L. Xiao, W. Chen, R.L. Mernaugh, H. Cai, K.E. Bernstein, et al. 2015. Immune activation caused by vascular oxidation promotes fibrosis and hypertension. *J. Clin. Invest.* 21:22–25.

Yang, L., M. Xie, M. Yang, Y. Yu, S. Zhu, W. Hou, R. Kang, M.T. Lotze, T.R. Billiar, H. Wang, et al.. 2014a. PKM2 regulates the Warburg effect and promotes HMGB1 release in sepsis. *Nat. Commun.* 5:4436. http://dx.doi.org/10.1038/ncomms5436

Yang, P., Z. Li, R. Fu, H. Wu, and Z. Li. 2014b. Pyruvate kinase M2 facilitates colon cancer cell migration via the modulation of STAT3 signalling. *Cell. Signal.* 26:1853–1862. http://dx.doi.org/10.1016/j.cellsig.2014.03.020

Yang, P., Z. Li, H. Li, Y. Lu, H. Wu, and Z. Li. 2015. Pyruvate kinase M2 accelerates pro-inflammatory cytokine secretion and cell proliferation induced by lipopolysaccharide in colorectal cancer. *Cell. Signal.* 27:1525–1532. http://dx.doi.org/10.1016/j.cellsig.2015.02.032

Yang, W., Y. Xia, D. Hawke, X. Li, J. Liang, D. Xing, K. Aldape, T. Hunter, W.K. Alfred Yung, and Z. Lu. 2012. PKM2 phosphorylates histone H3 and promotes gene transcription and tumorigenesis. *Cell.* 150:685–696. http://dx.doi.org/10.1016/j.cell.2012.07.018

Zhou, R., A.S. Yazdi, P. Menu, and J. Tschopp. 2011. A role for mitochondria in NLRP3 inflammasome activation. *Nature.* 469:221–225. http://dx.doi.org/10.1038/nature09663

Zou, C., Y. Wang, and Z. Shen. 2005. 2-NBDG as a fluorescent indicator for direct glucose uptake measurement. *J. Biochem. Biophys. Methods.* 64:207–215. http://dx.doi.org/10.1016/j.jbbm.2005.08.001